

**Matrix Isolation Infrared Spectroscopy and
Computational Study of complexes between
Phenylacetylene with Methanol and Methylamine**

By

MARIYAM FATIMA

*A dissertation submitted for the partial fulfilment of
BS-MS dual degree in Science*



Indian Institute of Science Education and Research Mohali

April 2014

Certificate of Examination

This is to certify that the dissertation titled “Matrix Isolation Infrared Spectroscopy and Computational Study of complex between Phenylacetylene-D with Methanol and Methylamine” submitted by Miss. Mariyam Fatima (Reg. No. MS09140) for the partial fulfilment of BS-MS dual degree programme of the Institute, has been examined by the thesis committee duly appointed by the Institute. The committee finds the work done by the candidate satisfactory and recommends that the report be accepted.

Dr. Sugumar

Dr. Ramesh Ramachandran

Prof. K.S. Viswanathan
(Supervisor)

Dated: April 25, 2014

DECLARATION

The work presented in this dissertation has been carried out by me under the guidance of Prof. K. S Viswanathan at the Indian Institute of Science Education and Research Mohali. This work has not been submitted in part or in full for a degree, a diploma, or a fellowship to any other university or institute. Whenever contributions of others are involved, every effort is made to indicate this clearly, with due acknowledgement of collaborative research and discussions. This thesis is a bonafide record of original work done by me and all sources listed within have been detailed in the bibliography.

Mariyam Fatima

(Candidate)

Dated: April 25, 2014

In my capacity as the supervisor of the candidate's project work, I certify above statements by the candidate are true to the best of my knowledge.

Prof. K.S. Viswanathan

(Supervisor)

ACKNOWLEDGEMENTS

I express my deep sense of gratitude and profound feeling of admiration to Prof. K. S. Viswanathan for his advice, expert guidance, valuable suggestions, discussions and constant encouragement during the entire course of this work and preparation of the thesis. I have really enjoyed the work under his guidance. I am also grateful to my Master's thesis committee members Dr. Sugumar and Dr. Ramesh Ramachandran for their valuable suggestions and comments during the committee meeting.

I am grateful to my lab members Kanupriya Verma, Ginny Karir, Jyoti Saini and Deepak Verma who accompanied me throughout this research work. I owe a special word of thanks to Dr. Bishnu Prasad Kar, Gaurav Kumar and Kapil Dave for helping me in carrying out the computational calculations and teaching the instrumentation technique.

I thank my friends Atul Mantri, Sapna Meena, Nishtha Agarwal, and all my batch mates who provided a wonderful and friendly atmosphere to carry out research during the entire period. It is my pleasure to thank each and every member of the Department of Chemical sciences who have helped me in various ways during the course of investigation and research.

I wish to acknowledge the Computing Facility staff for providing me excellent facilities during the computational work. I am extremely thankful to Prof. N. Sathyamurthy, Director, IISER Mohali, for allowing me to use the various facilities of this institute to carry out the research work.

I express my sincere gratitude to my cousin Dr. Mohammad Ali Haider who has guided me in various ways throughout my academic life, my parents Mr. K. Anwer and Mrs. Masarrat Anwer and my brother and sister for their encouragement and moral support throughout the course of study.

I would also like to acknowledge the 'Department of Science and Technology, India' and 'Indian Institute of Science, India' for providing the KVPY fellowship.

LIST OF FIGURES

Figure	Figure Caption	Pg.No
Figure 1.1	H-bonding sites in Phenylacetylene	4
Figure 1.2	Comparison of Phac and Phac-D spectra in Nitrogen	4
Figure 2.1	Representation of matrix isolated species in a host gas (clear circles). The rigid host isolates the various species from each other thereby preventing intermolecular interactions	7
Figure 2.2	Block diagram of Cryostat	12
Figure 2.3	Optical extension unit of Cryostat	12
Figure 2.4	Block diagram of Diffusion pump	13
Figure 2.5	Matrix Isolation Spectroscopy setup in IISER-Mohali	16
Figure 3.1	IR Spectra of Phac-D and Methanol in Nitrogen, the spectra spans the region from 2800-2400cm ⁻¹ and 900-700cm ⁻¹	28
Figure 3.2	IR Spectra of Phac-D and Methanol in Nitrogen, the spectra spans the region from 4000-3500cm ⁻¹	29
Figure 3.3	IR Spectra of Phac-D and Methanol in Argon, the spectra spans the region from 2800-2400cm ⁻¹ and 900-700cm ⁻¹	30
Figure 3.4	IR Spectra of Phac-D and Methanol in Argon, the spectra spans the region from 4000-3500cm ⁻¹	31
Figure 3.5	Complex structure between Phac-D and Methanol at B3LYP/6-311G++(d,p) with stabilization energy	33
Figure 3.6	Complex structure between Phac-D and Methanol at M062x/6-311G++(d,p) with stabilization energy	34

Figure 3.7	AIM analysis at B3LYP/6-311G++(d,p) level	45
Figure 3.8	AIM analysis at M062x/6-311G++(d,p) level	46
Figure 4.1	IR Spectra of Phac-D and Methylamine in Nitrogen, the spectra spans the region from 2800-2400cm ⁻¹ and 900-700cm ⁻¹	57
Figure 4.2	IR Spectra of Phac-D and Methanol in Nitrogen, the spectra spans the region from 4000-3500cm ⁻¹	58
Figure 4.3	IR Spectra of Phac-D and Methylamine in Argon, the spectra spans the region from 2800-2400cm ⁻¹ and 900-700cm ⁻¹	59
Figure 4.4	IR Spectra of Phac-D and Methanol in Argon, the spectra spans the region from 4000-3500cm ⁻¹	60
Figure 4.5	Complex structure between Phac-D and Methylamine at B3LYP/6-311G++(d,p) with stabilization energy	61
Figure 4.6	Complex structure between Phac-D and Methylamine at M062x/6-311G++(d,p) with stabilization energy	62
Figure 4.7	AIM analysis at B3LYP/6-311G++(d,p) level	76
Figure 4.8	AIM analysis at M062x/6-311G++(d,p) level	77

LIST OF TABLES

Table	Table Heading	Pg.No.
Table 3.1	Stabilization Energy for Phac-D and Methanol Complexes (Raw/ZP/BSSE)	32
Table 3.2	Some selected geometrical parameters of Complex 1 at B3LYP/6-311G++(d,p) and M062x/6-311G++(d,p) where bond length is given in Å , bond angle in degree(°) and torsional angles in degree(°)	35
Table 3.3	Some selected geometrical parameters of Complex 2 at B3LYP/6-311G++(d,p) and M062x/6-311G++(d,p) where bond length is given in Å , bond angle in degree(°) and torsional angles in degree(°)	36
Table 3.4	Some selected geometrical parameters of Complex 3 at B3LYP/6-311G++(d,p) and M062x/6-311G++(d,p) where bond length is given in Å , bond angle in degree(°) and torsional angles in degree(°)	37
Table 3.5	Some selected geometrical parameters of Complex 4 at M062x/6-311G++(d,p) where bond length is given in Å , bond angle in degree(°) and torsional angles in degree(°)	38
Table 3.6	Calculated and experimental frequency table for shifts in Phenylacetylene-D (Phac-D) C-D stretching due to the formation of Phenylacetylene-D and Methanol complexes in N ₂ matrix at B3LYP/6-311G++(d,p)	39
Table 3.7	Calculated and experimental frequency table for shifts in Phenylacetylene-D (Phac-D) C-D bending due to the formation	39

	of Phenylacetylene-D and Methanol complexes in N ₂ matrix at B3LYP/6-311G++(d,p)	
Table 3.8	Calculated and experimental frequency table for shifts in Phenylacetylene-D (Phac-D) C-D stretching due to the formation of Phenylacetylene-D and Methanol complexes in N ₂ matrix at M062x/6-311G++(d,p)	40
Table 3.9	Calculated and experimental frequency table for shifts in Phenylacetylene-D (Phac-D) C-D bending due to the formation of Phenylacetylene-D and Methanol complexes in N ₂ matrix at M062x/6-311G++(d,p)	40
Table 3.10	Calculated and experimental frequency table for shifts in Methanol O-H stretching frequency due to the formation of Phenylacetylene-D and Methanol complexes in N ₂ matrix at B3LYP/6-311G++(d,p)	41
Table 3.11	Calculated and experimental frequency table for shifts in Methanol O-H stretching frequency due to the formation of Phenylacetylene-D and Methanol complexes in Argon matrix at M062x/6-311G++(d,p)	41
Table 3.12	Calculated and experimental frequency table for shifts in Phenylacetylene-D (Phac-D) C-D stretching due to the formation of Phenylacetylene-D and Methanol complexes in Argon matrix at B3LYP/6-311G++(d,p)	42
Table 3.13	Calculated and experimental frequency table for shifts in Phenylacetylene-D (Phac-D) C-D bending due to the formation of Phenylacetylene-D and Methanol complexes in Argon matrix at B3LYP/6-311G++(d,p)	42
Table 3.14	Calculated and experimental frequency table for shifts in Phenylacetylene-D (Phac-D) C-D stretching due to the formation of Phenylacetylene-D and Methanol complexes in Argon matrix at M062x/6-311G++(d,p)	43
Table 3.15	Calculated and experimental frequency table for shifts in Phenylacetylene-D (Phac-D) C-D bending due to the formation	43

	of Phenylacetylene-D and Methanol complexes in Argon matrix at M062x/6-311G++(d,p)	
Table 3.16	Calculated and experimental frequency table for shifts in Methanol O-H stretching frequency due to the formation of Phenylacetylene-D and Methanol complexes in Argon matrix at M062x/6-311G++(d,p)	44
Table 3.17	Calculated and experimental frequency table for shifts in Methanol O-H stretching frequency due to the formation of Phenylacetylene-D and Methanol complexes in Argon matrix at M062x/6-311G++(d,p)	44
Table 3.18	Properties of different critical points present in Phac-D and Methanol complexes as a result of AIM analysis in B3LYP/6-311G++(d,p)	47
Table 3.19	Properties of different critical points present in Phac-D and Methanol complexes as a result of AIM analysis in M062x/6-311G++(d,p).	47
Table 4.1	Stabilization Energy for Phac-D and Methylamine Complexes (Raw/ZP/BSSE)	56
Table 4.2	Some selected geometrical parameters of Complex 1 at B3LYP/6-311G++(d,p) and M062x/6-311G++(d,p) where bond length is given in Å , bond angle in degree(°) and torsional angles in degree(°)	63
Table 4.3	Some selected geometrical parameters of Complex 2 at B3LYP/6-311G++(d,p) and M062x/6-311G++(d,p) where bond length is given in Å , bond angle in degree(°) and torsional angles in degree(°)	64
Table 4.4	Some selected geometrical parameters of Complex 3 at B3LYP/6-311G++(d,p) and M062x/6-311G++(d,p) where bond length is given in Å , bond angle in degree(°) and torsional angles in degree(°)	65
Table 4.5	Calculated and experimental frequency table for shifts in Phenylacetylene-D (Phac-D) C-D stretching due to the	66

	formation of Phenylacetylene-D and Methylamine complexes in N ₂ matrix at B3LYP/6-311G++(d,p)	
Table 4.6	Calculated and experimental frequency table for shifts in Phenylacetylene-D (Phac-D) C≡C stretching due to the formation of Phenylacetylene-D and Methylamine complexes in N ₂ matrix at B3LYP/6-311G++(d,p)	66
Table 4.7	Calculated and experimental frequency table for shifts in Phenylacetylene-D (Phac-D) C-D bending due to the formation of Phenylacetylene-D and Methylamine complexes in N ₂ matrix at B3LYP/6-311G++(d,p)	67
Table 4.8	Calculated and experimental frequency table for shifts in Phenylacetylene-D (Phac-D) C-D stretching due to the formation of Phenylacetylene-D and Methylamine complexes in N ₂ matrix at M062x/6-311G++(d,p)	68
Table 4.9	Calculated and experimental frequency table for shifts in Phenylacetylene-D (Phac-D) C≡C stretching due to the formation of Phenylacetylene-D and Methylamine complexes in N ₂ matrix at M062x/6-311G++(d,p)	68
Table 4.10	Calculated and experimental frequency table for shifts in Phenylacetylene-D (Phac-D) C-D bending due to the formation of Phenylacetylene-D and Methylamine complexes in N ₂ matrix at M062x/6-311G++(d,p)	69
Table 4.11	Calculated and experimental frequency table for shifts in Methylamine N-H bending frequency due to the formation of Phenylacetylene-D and Methylamine complexes in N ₂ matrix at B3LYP/6-311G++(d,p)	70
Table 4.12	Calculated and experimental frequency table for shifts in Methylamine N-H bending frequency due to the formation of Phenylacetylene-D and Methylamine complexes in N ₂ matrix at M062x/6-311G++(d,p)	70
Table 4.13	Calculated and experimental frequency table for shifts in Phenylacetylene-D (Phac-D) C-D stretching due to the	71

	formation of Phenylacetylene-D and Methylamine complexes in Ar matrix at B3LYP/6-311G++(d,p)	
Table 4.14	Calculated and experimental frequency table for shifts in Phenylacetylene-D (Phac-D) C≡C stretching due to the formation of Phenylacetylene-D and Methylamine complexes in Ar matrix at B3LYP/6-311G++(d,p)	71
Table 4.15	Calculated and experimental frequency table for shifts in Phenylacetylene-D (Phac-D) C-D bending due to the formation of Phenylacetylene-D and Methylamine complexes in Ar matrix at B3LYP/6-311G++(d,p)	72
Table 4.16	Calculated and experimental frequency table for shifts in Phenylacetylene-D (Phac-D) C-D stretching due to the formation of Phenylacetylene-D and Methylamine complexes in Ar matrix at M062x/6-311G++(d,p)	73
Table 4.17	Calculated and experimental frequency table for shifts in Phenylacetylene-D (Phac-D) C≡C stretching due to the formation of Phenylacetylene-D and Methylamine complexes in Ar matrix at M062x/6-311G++(d,p)	73
Table 4.18	Calculated and experimental frequency table for shifts in Phenylacetylene-D (Phac-D) C-D bending due to the formation of Phenylacetylene-D and Methylamine complexes in Argon matrix at M062x/6-311G++(d,p)	74
Table 4.19	Calculated and experimental frequency table for shifts in Methylamine N-H bending frequency due to the formation of Phenylacetylene-D and Methylamine complexes in Argon matrix at B3LYP/6-311G++(d,p)	75
Table 4.20	Calculated and experimental frequency table for shifts in Methylamine N-H stretching frequency due to the formation of Phenylacetylene-D and Methylamine complexes in Ar matrix at M062x/6-311G++(d,p)	75
Table 4.21	Properties of different critical points present in Phac-D and Methylamine complexes as a result of AIM analysis in B3LYP/6-311G++(d,p)	78

Table 4.22 Properties of different critical points present in Phac-D and Methylamine complexes as a result of AIM analysis in M062x/6-311G++(d,p).

78

LIST OF NOTATIONS

Phac	Phenylacetylene
Phac-D	Phenylacetylene-D
IR	Infrared
UV	Ultra Violet
Vis	Visible
Elec	Electrostatic
Ind	Inductive
Dis	Dispersive
Rep	Repulsive
KBr	Potassium bromide
HF	Hartree-Fock
DFT	Density Functional Theory
CI	Configuration interaction
CC	Coupled cluster
BLYP	Becke-Lee-Yang-Parr
B3LYP	3 parameters used in the function
M06	Minnesota functional
ZPE	Zero point vibrational energy
BSSE	Basis Set Superposition Error
AIM	Atoms-in-molecules
CP	Critical point
BCP	Bond Critical Point

CONTENT

	P.N.
List of Figures	i
List of Tables	iii
List of Notations	ix
Abstract	xii
CHAPTER 1 INTRODUCTION	1
1.1 Hydrogen Bonding	1
1.2 Present work	3
CHAPTER 2 EXPERIMENTAL AND COMPUTATIONAL PROCEDURE	5
2.1 Matrix Isolation Infrared Spectroscopy	5
2.2 Advantages of Matrix Isolation technique	7
2.3 Matrix Effects	8
2.4 Matrix Isolation Infrared Setup	9
2.5 Experimental Procedure	14
2.6 Computational Details	15
2.6.1 Structure Optimization	15
2.6.2 Basis set	17
2.6.3 Level of Theory	17
2.6.4 Energy Calculations	18
2.6.5 Atoms in Molecules	20

CHAPTER 3	STUDY ON THE COMPLEX FORMATION OF PHENYLACETYLENE-D AND METHANOL	21
	3.1 Experimental	21
	3.2 Computation	22
	3.3 Vibrational Assignment	23
	3.4 Atoms in Molecules Study	27
	3.5 Conclusion	27
CHAPTER 4	STUDY ON THE COMPLEX FORMATION OF PHENYLACETYLENE-D AND METHYLAMINE	48
	4.1 Experimental	48
	4.2 Computation	49
	4.3 Vibrational Assignment	50
	4.4 Atoms in Molecules Study	54
	4.5 Conclusion	55
CHAPTER 5	SUMMARY AND CONCLUSIONS	79
	5.1 Scope for Future Work	80
	BIBLIOGRAPHY	81

ABSTRACT

Hydrogen bond is a unique interaction which has important ramifications in chemical and bio-chemical reactions including life processes. It comes under the class of non-covalent interactions. In spite of this concept being about a century old and extensive work being done in this area, the concept of hydrogen bonding is still not completely understood. Starting from the conventional type of hydrogen bonding to the discovery of non-conventional types, the definition of hydrogen bonding is continuously expanding.

There are many experimental methods such as infrared spectroscopy, NMR etc. that are available to study hydrogen bonding interactions. In the present work we have combined infrared spectroscopy with the Matrix Isolation technique for hydrogen bonding studies, as this technique serves as a powerful tool to study weak interactions. In this method the molecules are trapped at low temperature which results in sharp spectral feature and hence permits the resolution of features of the complexes formed in the matrix.

In this work, we studied the hydrogen bonding interaction between phenylacetylene with methanol and methylamine. Phenylacetylene is an ideal molecule as it contains multiple hydrogen bonding sites; it can act as proton donor or proton acceptor. We have taken methanol and methylamine as we want to study the preferred hydrogen bonding interaction of phenylacetylene when we switch from O-H to N-H group.

The computation work have been performed at B3LYP and M06-2x level of theories using 6-311G++(d,p) basis set. For the phenylacetylene-methanol complexe, three different geometries at B3LYP and four at M06-2x were obtained. In the case of phenylacetylene-methylamine complex, three different geometries were obtained at both levels of theory. Computationally, at the B3LYP level, C-H...O and C-H...N interaction has been observed to be dominant. At M06-2x, O-H... π and N-H... π have been observed as dominant interaction. However, experimental studies have shown that C-H...O, O-H... π and C-H...N as the dominant interaction.

Chapter 1

INTRODUCTION

1.1 Hydrogen Bonding

The hydrogen bond is of great importance in many fields [1]. It is weaker than chemical bond, and is observed in solid, liquid and gases. These bonds are represented as X-H...Y, where X and Y are atoms having higher electronegativity than Hydrogen (e.g. O, N, F, Cl, S). In this the hydrogen atom H is non-covalently bonded to the neighbouring acceptor atom Y [2]. The H-X group is called the 'H bond donor' and the Y group is called 'H bond acceptor'.

This is the classic or conventional definition of hydrogen bond. But there have been examples of unconventional interactions. The C-H group interaction with oxygen was first proposed in 1960s [3, 4]. The concept of dihydrogen bond was also introduced [5-7]. In 1998, 'anti-hydrogen bond' was identified in benzene dimer and other benzene complexes which was later called blue shifts in hydrogen bond as it was due to C-H bond shortening and a blue shift in C-H stretching frequency [8]. π ...H+... π interactions [9] and monoelectron dihydrogen interaction, H...e...H [10, 11] have also been proposed.

Therefore, another definition of hydrogen bonding, based on van der Waals interactions, is: [12]

“A hydrogen bond exists between the functional group X-H, and an atom or a group of atoms, Y, in the same or different molecules when 1) there is an evidence of bond formation and, in 2) this new bond linking X-H and Y specifically involves a hydrogen atom already bonded to X”.

H-bonding is highly electrostatic and partly covalent interaction and has contributions from electrostatic interactions, polarization effects, van der Waals interactions and covalence [13]. The hydrogen bond energies cover the range between 0.2 to 40 kcal mol⁻¹.

1.1.1 Nature of Hydrogen Bond

It has been shown that the formation of X–H...Y bond is accompanied by a weakening of the covalent X–H bond with decrease of X–H stretching frequency [14, 15]. This red shift is an important characteristics of the H-bonding interaction. Another feature of H bonding is the considerable increase in the intensity of the spectral band associated with X–H stretching frequency, which leads to a non-negligible electron density transfer from a proton acceptor to a donor [16]. Electron density is transferred from the proton acceptor (lone pair) to the sigma- anti-bonding orbital of X–H bond, which causes a weakening and elongation of this bond and a decrease in the X–H stretch frequency. On the contrary, there are some typical situations, wherein the X–H bond gets compressed and the corresponding X–H stretching vibration is shifted to a higher frequency. This type is called as blue shifted H-bond or improper or anti-H bond.

1.1.2 Study on Hydrogen bonding

There have been numerous experimental studies on hydrogen bonding. Infrared (IR) and nuclear magnetic resonance (NMR) techniques have been widely used to analyse H-bonding interactions in many systems [14, 15, 17]. Spectroscopic information obtained from these techniques has been used to probe H-bonding interactions.

Some of the other techniques that are being used to probe the noncovalent interactions are microwave, vibrational rotation tunneling (VRT), REMPI and hole burning, and zero kinetic energy (ZEKE) [17].

Theoretical methods using quantum chemistry have also been used to analyse H-bonding interactions. (These are not semi-empirical methods) Quantum chemical methods such as Hartree–Fock (HF), and post-HF methodologies have been employed to study H-bonding. Møller–Plesset (MP2), coupled-cluster singles doubles (CCSD) and DFT methods are widely used methodologies to investigate H-bonding interactions. The basis set used in the calculation influences the calculated bond length, bond angle, electronic properties, interaction energy, and vibrational spectra [18]. Therefore, theoretically, different

combinations of theories and basis sets are applied to obtain estimate of geometrical parameters and energetics of H-bonded systems.

1.2 Present Work

In this work, the multiple binding sites of a phenylacetylene provides the possibility to investigate competitive hydrogen bonding. Usually, the multiple hydrogen bonding sites throws up a competition between electrostatic and dispersion energy terms in order to maximize the interaction energy.

Phenylacetylene (Phac), Fig 1.1, is a molecule which contains multiple hydrogen bonding sites which can switch from electrostatic to dispersion interactions. The sites present in Phac are (A) acetylenic C-H, this site can act as hydrogen donor site, (B) acetylenic π cloud as hydrogen acceptor and (C) benzene π cloud as hydrogen acceptor.

In this work the possibility of Hydrogen bonded complex formation between Phenylacetylene (Phac) with Methanol and Methylamine have been studied to understand the nature of hydrogen bonding when switching from O-H to N-H group. Although this work has been reported earlier[19] using gas phase studies, we undertook the study of this system in the matrix as the matrix isolation technique can locate local minima other than only global minima.

In this work, Phenylacetylene-D (Phac-D) has been used instead of Phac because Phac has features at 3322.6 and 3309 cm^{-1} as shown in Fig 1.2, which have been assigned to a Fermi diad comprising of $\text{C}\equiv\text{C}$, C-H stretching and C-H bending [20]. This presence of a diad of features, makes the identification of features due to the complexes. Hence we used Phac-D, in which the Fermi resonance is suppressed.

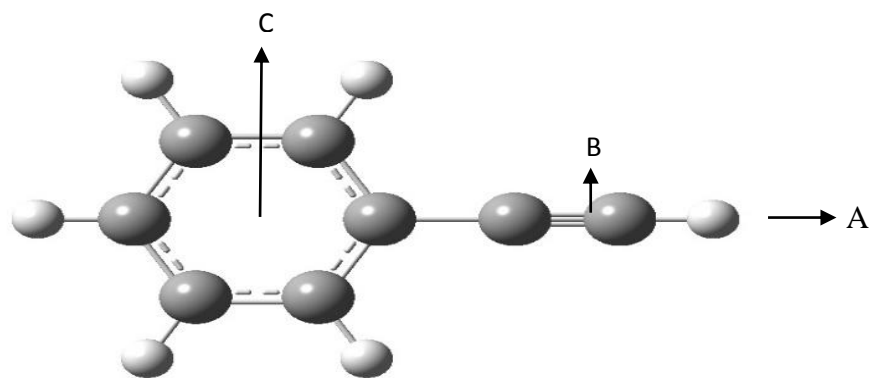


Fig 1.1 H-bonding sites in Phenylacetylene

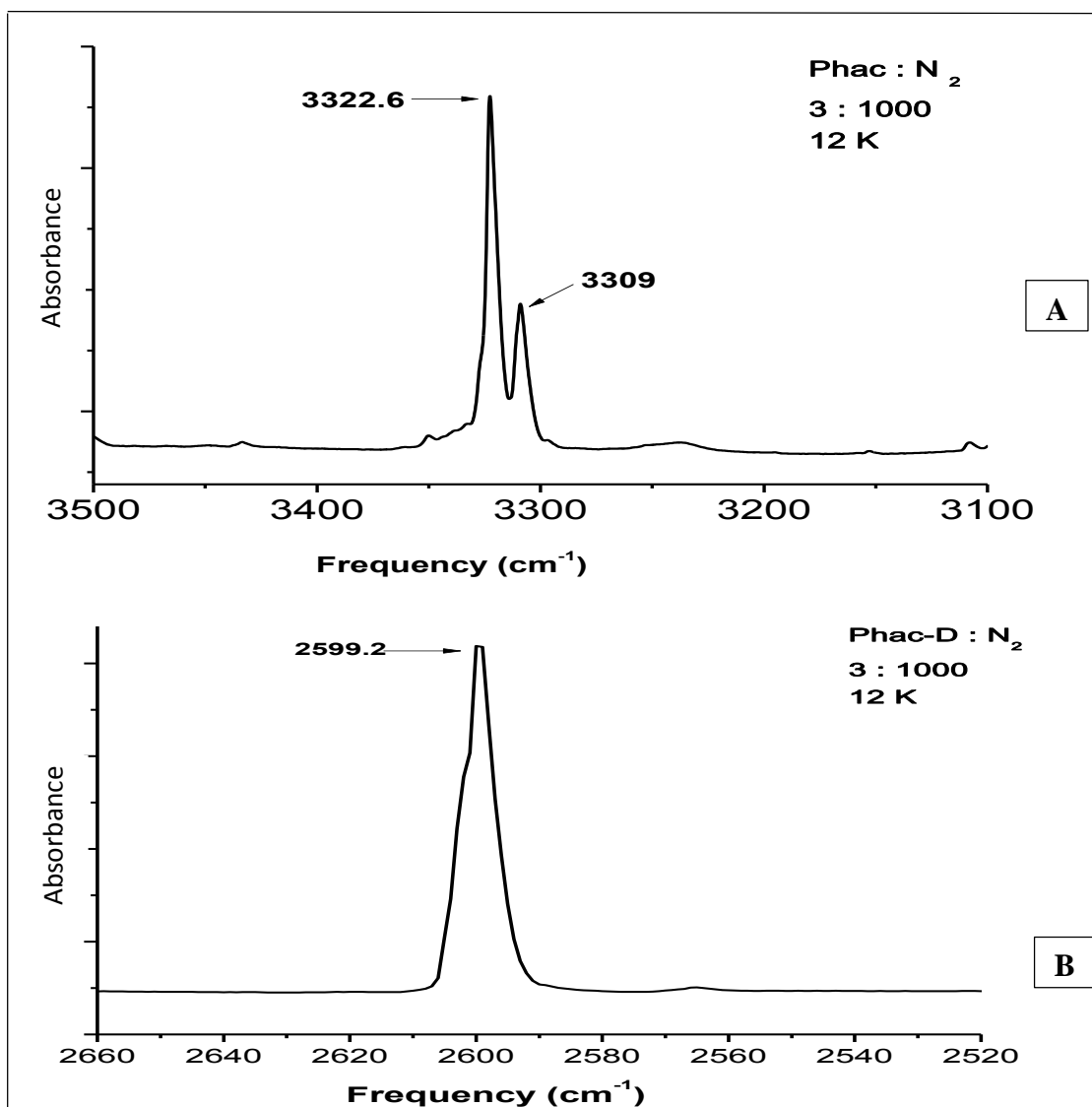


Fig 1.2 : Comparison of the IR spectra of Phac and Phac-D, A) IR Spectra of Phenylacetylene in nitrogen at 12K, and B) IR Spectra of Phenylacetylene-D in nitrogen at 12K

Chapter 2

EXPERIMENTAL AND

COMPUTATIONAL PROCEDURE

Matrix Isolation Spectroscopy is a technique in which the molecules of interest are isolated in an inert matrix which is then probed using a variety of spectroscopic techniques. The matrix is usually an inert gas which presents a rigid environment for the molecules to produce the solid matrix, it is necessary to maintain the temperature of the system very low (~12K). In the following discussions we have used Fourier Transform Infrared Spectroscopy (FTIR) to study the interactions between Phenylacetylene-D and Methanol; and Phenylacetylene-D and Methylamine.

2.1 Matrix Isolation Infrared Spectroscopy:

Matrix Isolation (MI) is essentially a technique which deals with “low-temperature spectroscopy in rigid media” [21]. This technique was first invented by Pimental and co-workers [22] in 1954 to study chemical reactions between free radicals suspended in matrices at cryogenic temperatures. Matrix Isolation technique is now widely used to study unstable molecules generated by photolysis or gas phase thermolysis, to observe directly reaction intermediates, to generate and to study novel reactive species, to determine the structures of reactive species, to study particular molecular conformations and weak intermolecular interactions such as hydrogen bonding, and van der Waals complexes[23]. The Infrared (IR) bands of the submolecules in these complexes are perturbed which provides insight into the nature of intermolecular interactions.

The matrices are formed, using a non-reactive substance such as rare gases or solid nitrogen where the interaction between the sample and inert gas is negligible. The low temperatures required are achieved by cryostats with closed helium cycles in which the temperature can reach up to 4K.

Matrix isolation technique is a method for trapping molecules of interest in a host matrix in a very dilute and low temperature conditions to minimize any reaction between isolated molecules, resulting in molecules that are spatially separated while embedded into the matrix lattice. The matrix is prepared by first mixing the sample and the inert gas in a container maintained under vacuum, and then this mixture is condensed onto a cooled spectroscopic window (i.e. CsI or KBr for IR spectroscopy and a quartz or sapphire window for UV/Vis spectroscopy) through a nozzle.

Once the matrix has been formed, diffusion of molecular species is prevented as long as low temperatures are maintained. A matrix is considered to be rigid as long as the temperature is 30% of its freezing point. For example, if argon is used as the host gas, the temperature would have to be kept below 25K (since the freezing point of argon is 83.9K and $0.3 \times 83.9 = 25$) in order to ensure the rigidity of the matrix. The low temperature to obtain a rigid matrix ensures that bimolecular reactions through diffusion do not take place. Furthermore, because such low temperatures must be used, even modest reaction barriers prove to be substantially large as there is minimal thermal energy available to overcome them. As a result even very thermodynamically and kinetically favourable unimolecular dissociations become insignificant once the matrix has been formed. In case, one wishes to promote diffusion and to initiate further reaction, the matrix is slightly warmed and maintained at this elevated temperature, a process called annealing.

In order to characterize matrix isolated species, infrared, Ultraviolet-Visible (UV/VIS), and Electron Spin Resonance (ESR) spectroscopy are frequently used. In this study we have used Infrared (IR) spectroscopy to investigate the matrix isolated species. As the rotations in solid matrices are suppressed, the IR spectra shows very narrow and resolved peaks, which is not possible at room temperature IR spectra where all the possible ro-vibrational transition occurs resulting in broad peaks.

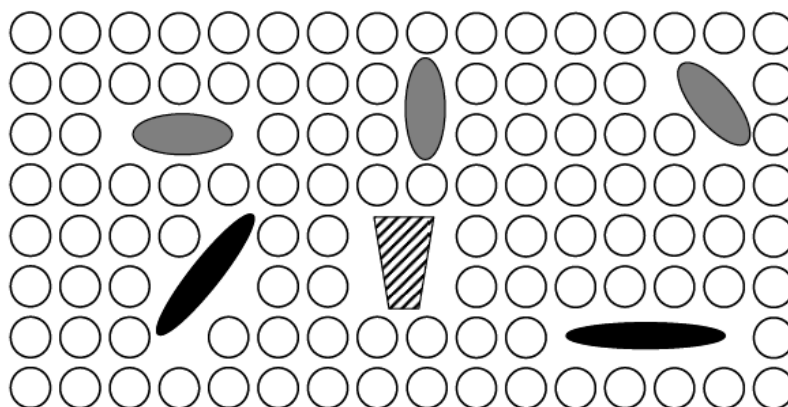


Fig 2.1: Representation of matrix isolated species in a host gas (clear circles). The rigid host isolates the various species from each other thereby preventing intermolecular interactions [24]

2.2 Advantages of Matrix Isolation:

1. The inert gases used as matrix material are nearly ideal for its use. They are mostly monoatomic except nitrogen which is diatomic so that they do not have any vibrations or change in dipole which can lead to IR spectra. This leads to optical transparency of the matrix in IR region.[25]
2. Broadening due to collision and Doppler effect are absent. The low temperature in the matrix also ensures that only low ro-vibronic and electronic levels of the samples are populated which results in significant reduction of spectral congestion and so we observe narrow peaks in IR spectra.
3. As this technique can trap the molecules, reactions in which intermediates cannot be directly observed due to short life of few micro seconds can be successfully isolated and characterized.
4. Trapping of molecules also helps in catching the different conformations possible in a structure. It helps in studying structures which are not possible to study using different techniques.

Apart from the various advantages of using Matrix Isolation, there are some features in the spectra due to matrices. These features are also called as Matrix effect and have been discussed below.

2.3 Matrix Effect

This feature arises because the matrix crystallizes in a face centered cubic (fcc) lattice (as known from the X-Ray diffraction method) [26]. In this unit cell each atom is surrounded by 12 nearest neighbours. This lattice contains two interstitial sites, Tetrahedral and Octahedral site.

The sample molecule can occupy any of these sites depending on its size or, it can also replace one or more of the host atom site leading to single or multiple substitutional sites. The sample molecules can occupy any of these sites depending on its size and so experiences different external field or constrain. This effect is known as multiple trapping site effect. This may lead to shifts in the normal modes or splitting of the band due to different interaction of molecules in different trapping sites.

There are also other kinds of matrix effects discussed further.

2.3.1 Perturbation of vibrational modes

The frequency shift, $\Delta\nu$ in a matrix with respect to the gas phase value arises from electrostatic ($\Delta\nu_{elec}$), inductive ($\Delta\nu_{ind}$), dispersive ($\Delta\nu_{dis}$) and repulsive interactions ($\Delta\nu_{rep}$) with the matrix molecules, and is given by the expression [27],

$$\Delta\nu = (\nu_{matrix} - \nu_{gas}) = \Delta\nu_{elec} + \Delta\nu_{ind} + \Delta\nu_{dis} + \Delta\nu_{rep} \dots\dots\dots (2.1)$$

Where ν_{matrix} and ν_{gas} are the frequencies of the vibrational mode of a molecule in the matrix and gas phase respectively.

In inert gas and in nitrogen, these shifts are usually small due to very weak interactions where the long range London dispersion forces and the short range repulsive forces are the two dominant interactions. A theoretical treatment of a matrix induced frequency shift has been given by Pimentel and Charles [28]. It has been shown that a tight cage usually introduces a blue shift in the vibrational frequencies (relative to the gas phase values) and a loose cage a red shift.

2.3.2 Rotation of molecules in matrix cage

Depending on the size of the molecule and the interstitial site, the molecules can rotate freely if the site is greater than the molecule. Generally in case of small molecules occupying interstitial sites in Ne, Ar, Kr or Xe, the rotational spectra have been observed [29-32]. For example, evidence has been presented that ammonia and water molecules rotate in an argon matrix but not in a nitrogen matrix [25]. The rotational features are identified by reversible intensity changes on temperature cycling, as opposed to splitting due to matrix site effects which are not reversible on temperature cycling.

2.3.3 Aggregation

In order to achieve complete isolation of the molecules to inhibit any intermolecular interactions, the molecules are trapped in the matrix gas such that they are far away from each other. The ratio of matrix : sample required for a complete isolation to occur is given by the probability of finding another molecule occupying one of the 12 sites that form the cage in the matrix. The chance for absence of second sample molecule to be the next nearest neighbour is given by the formula $P = (1-r)^{12}$, where r is the reciprocal of the matrix ratio. For very small value of r the expression becomes $P = (1-12r)$, from this it is clear that the matrix ratio of 1000 is needed to ensure 99% isolation.

As the solute concentration in the matrix increases, molecular aggregation such as dimers, trimers and multimers may be produced in addition to the monomers. The feature due to aggregation or self-association are generally identified by performing concentration dependence and warm-up experiments in which monomers diffuse to form dimers and higher multimers. Modification in vibrational band can also be observed if two species are trapped very nearby resulting in overlap of their respective cages.

2.4 Matrix Isolation Infrared Setup

The main component of the MI setup involves:

1. Cryostat
2. Vacuum system

3. FTIR spectrometer

2.4.1 Cryostat

Cryostats are used for the cooling of the trapping surface by utilizing the Joule-Thomson effect by the expansion of He or H₂ gas at high pressure [33]. Most of the matrix gases like Ar, Xe, Kr, Ne or N₂, requires a cooling temperature of around 10-15K for forming a solid matrix on the trapping surface. Therefore, the common cryogenic fluids that are used in cryostat to obtain low temperature are liquid He (bp=4.2K), liquid hydrogen (bp=20.4K) and liquid N₂ (bp=77.4K). A block diagram of a cryostat is shown in Fig 2.2.

The cryostat can be subdivided into five main sections [34]

- a. Cold head,
- b. A helium compressor,
- c. Temperature control unit,
- d. An optical extension set, and
- e. Trapping surface

In the first two sections (a & b), cold head, also referred as expander in the Gifford-McMahon refrigeration cycle, is the basic unit of the closed cycle cryostat. It is connected to a compressor by two gas lines. The working of the two gas lines is quite opposite in the sense that one of the gas lines is used to supply high pressure helium gas to the expander due to which the pressure differential drives the displacer allowing the expansion and cooling of the gas at the bottom, which later provides the low temperature at the cold head. Whereas, the other line returns the low pressure helium gas from the expander allowing the cold gas to flow and remove the heat from the system. The compressor provides the necessary helium gas flow rate at the high pressure for the expander to convert into the desired refrigeration capacity.

(c), the temperatures above 12 K can be obtained using a heater coil mounted on the cold tip. The temperature controller unit operates via regulating the current through the heater. This arrangement helps to obtain quite a lot of variation in the temperature ranging from 12 K to 300 K. To anneal the matrix, temperatures above 12 K is necessary which enhances the diffusion and promotes the reaction of the trapped species. Annealing is also done to examine the presence of multiple sites arising from unstable matrix sites. In our cryostat, the temperature is measured with the help of silicon diode sensor.

The final section of the cryostat, (d), i.e. the Optical extension unit comprises of a substrate holder, a radiation shield and a vacuum jackets as shown in Fig 2.6. The substrate holder is attached to the cold head of the cryostat, which attains a temperature of 12 K. A KBr (Potassium Bromide) substrate of 25 mm diameter and 4 mm thickness was mounted on the substrate holder and a radiation shield made up of copper is fixed around the cryotip. The rotatable vacuum jacket has four ports which is attached to another vacuum jacket through 'O' ring seal. A KBr window transmitting the infrared beam to the detector were mounted on two opposite ports of the rotatable vacuum jackets. The third port is fitted with a quartz window for viewing purposes and when required to transmit UV-visible light to study the effect of photo irradiation on the matrix isolated sample. To the fourth port, a sample inlet system is connected, through which deposition is conducted.

(e) Trapping Surface: The trapping surface for different spectroscopic regions are the crystalline forms of quartz or Si(far-IR), CsI, KBr, NaCl(IR), quartz, LiF (to 1050Å), CaF₂ (visible, UV), and sapphire rod or other non-conducting material for ESR spectra. Most of the study utilizes these windows which have low thermal conductivity. Although metal surfaces can also be used as they cover wider spectral range and also provide good thermal and light reflection properties [33].

In our experiments we have used KBr window as the trapping surface.

2.4.2 Vacuum System

There are two types of pumping system used in this setup.

a. Rotary pump :

Rotary pumps are also known as Mechanical pumps as they physically sweep the air from the system, usually with a rotary device. The rotor is eccentric to the pump cavity. The rotating vane is kept in contact with the walls of the pump cavity by means of a compression spring. Rotating vane, positive displacement pumps have large gas handling capacities, but cannot achieve high vacuum. The average vacuum attained by rotary pump is around 10^{-3} torr.

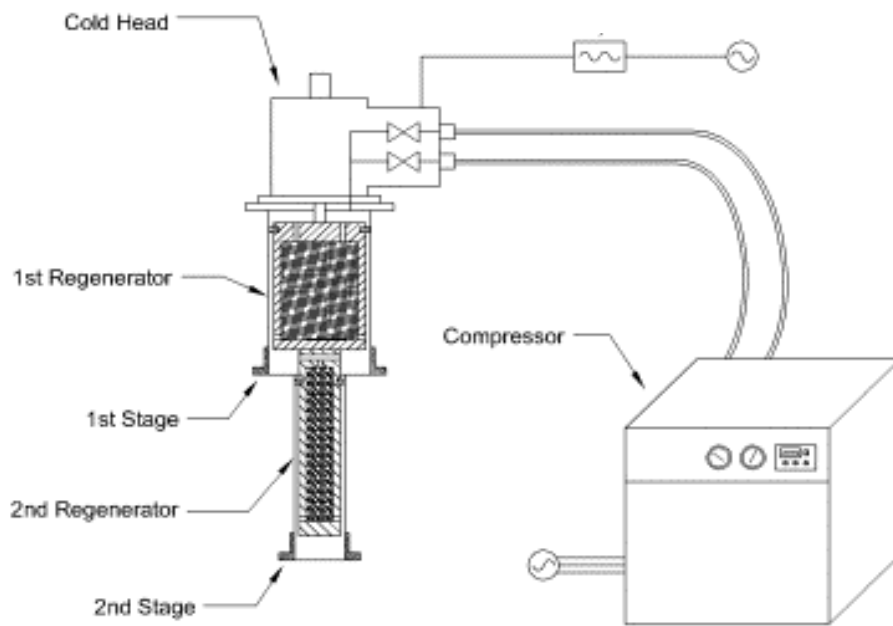


Fig 2.2 Block diagram of Cryostat [35]

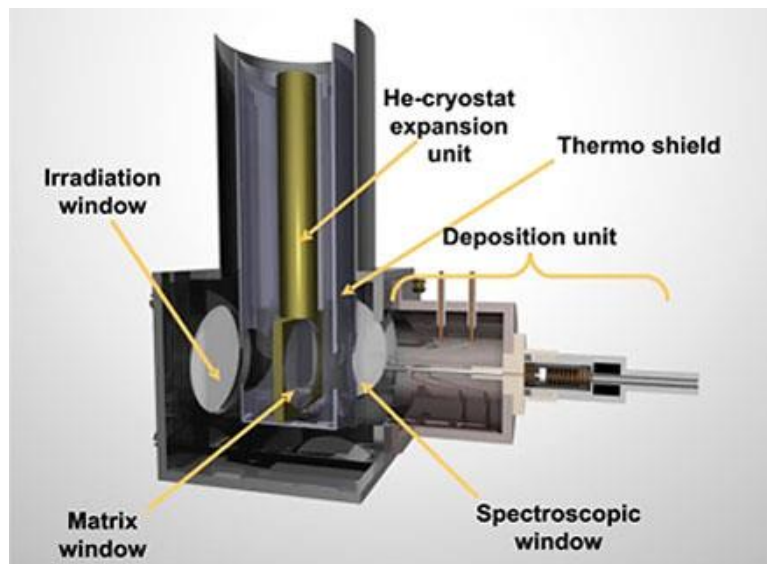


Fig 2.3 Optical extension unit of Cryostat [36]

These pumps are preferably used for two purposes: (a) to remove (rough) the bulk of the air from a system which is initially at atmospheric pressure, and, (b) to back the diffusion pump, since diffusion pump cannot exhaust against atmospheric pressure [37].

The rotary pump used in this setup has a pumping speed of 100 litre/min. There are two rotary pumps used, one for backing up the diffusion pump and the second as a roughing pump for the vacuum system.

b. Diffusion Pump :

A vacuum diffusion pump is made of a stainless steel chamber containing vertically stacked cone-shaped jet assemblies. At the base of the chamber there is a specialized type of oil having a low vapour pressure, and this oil is heated to boiling by an electric heater at the base of the chamber. The vaporized oil then moves upward and is expelled through the jets in the various assemblies as shown in the Fig 2.7. To cool the chamber, cold water from the chiller is circulated through the coils on the outside of the chamber [38].

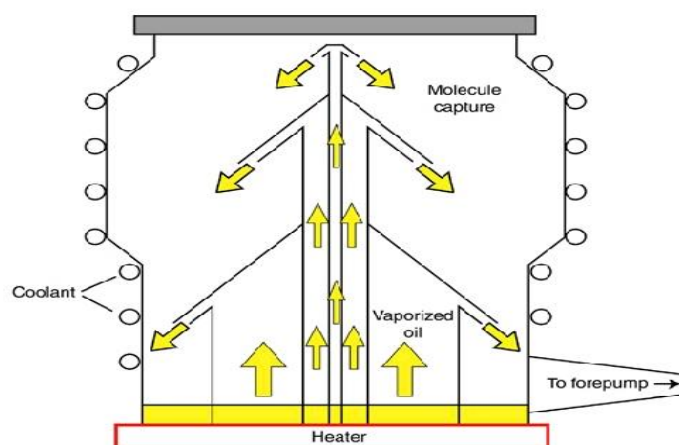


Fig 2.4 Block diagram of Diffusion pump [38]

An oil diffusion pump with a pumping speed of 280 litre/lit has been used in this setup, backed by a rotary pump. A butterfly valve has been used to isolate the cryostat from the diffusion pump. The base vacuum in the system is around $\sim 10^{-6}$ torr, which is measured using a cold cathode gauge.

There are other types of high vacuum pumps available like cryopumps and ion pumps, but diffusion pump is generally used for this technique because of several advantages: they are reliable, they are simple in design, they run without noise or vibration, and they are

relatively inexpensive to operate and maintain. These pumps also tolerate operating conditions such as excess particles and reactive gases that would destroy other types of high vacuum pumps.

2.4.3 FTIR Spectrometer

To investigate the matrix, as mentioned in the previous section there are many spectroscopic methods available. In this setup we have used Fourier transformed infrared Spectroscopy (FTIR) to determine the structure of the complex formed. As most of the rotational bands are suppressed under cryogenic temperatures, the IR spectra recorded under these conditions shows a very narrow peak compared to many overlapping vibration and rotation modes in spectra at room temperature.

A Perkin Elmer FTIR spectrometer has been used in this setup having a resolution of 1cm^{-1} .

2.5 Experimental Procedure

A mixture of analyte and matrix host was prepared by premixing them in a stainless steel mixing chamber of one liter capacity, which was introduced to the vacuum system through a single effusive nozzle.

The samples Phenylacetylene-D (Phac-D) (Sigma Aldrich, 99% D), Methanol (Central Drug House, 99.5%), and Methylamine (Sigma Aldrich, 40 wt. % in H_2O), were used and two different host matrix gas, N_2 and Ar were used for this study. Samples were loaded in the glass bulbs connected to the mixing chamber through high vacuum glass stopcocks, which were thoroughly degassed for several hours before the samples are loaded in them and the samples are then subjected to several freeze-thaw-pump cycles to remove any impurity. These samples are liquids of high vapour pressure; hence the samples were equilibrated at the required temperature, for about an hour, using an ethanol-liquid nitrogen slush bath, to obtain the desired vapour pressure over the sample. The temperature of the slush bath was measured using a platinum resistance thermometer. The desired matrix/sample ratios were thus obtained by controlling the vapour pressure over the sample. The mixture was prepared in the mixing chamber and then allowed to deposit on the cold KBr substrate through the nozzle. Deposition rate ($\sim 3\text{mmol}/\text{hour}$) is controlled through a

fine needle valve. Around 80-100 mtorr is deposited on the substrate for a thin and uniform pellet to form.

Then the Infrared Spectra are recorded using FTIR spectrometer with a spectral resolution 1 cm^{-1} . The matrix are then annealed at different temperatures, and the IR spectra are again recorded.

2.6 Computational Details

Computational chemistry has become a major tool to investigate a variety of chemical problems such as molecular geometry, reactivity, infrared spectra, and the physical properties of molecules. There are many theories available to calculate the molecular parameters to a good approximation. The combination of these theories along with different types of basis set are used for calculations of different system.

In this work the use of computational calculation was used to predict the complexes where the vibrational modes of those molecules were calculated and used as a guide in the analysis of the spectra. In this work Gaussian 09 [39] was used for all calculations. Additionally GaussView5 was used both to create input structures and to visualize the optimized structures and their various vibrational modes. In all cases density functional theory was used with the restricted B3LYP functional and M062x with a 6-311G++(d,p) basis set.

2.6.1 Structure Optimization:

Structure optimization method find a stationary point on the Potential Energy Surface (PES) that is, it finds a minimum, or a saddle point for a specific structure [40]. The calculation for optimization is done by calculation of the possible geometric parameters and then finding the derivative of energy with respect to these parameters. When with respect to all parameters the derivative of energy is zero then the stationary point is reached and at that structure, energy and frequency are



Fig 2.5: Matrix Isolation Spectroscopy setup in IISER-Mohali

calculated. Therefore, the optimized structure that is located depends on the input geometry, as the algorithm tries to find the nearest stationary point to the input geometry; hence, if one starts with a geometry that is very near a transition state (TS) structure, the optimization procedure may converge to that structure. [41]

2.6.2 Basis set

The basis set gives the mathematical description of the orbitals. The orbitals are built of linear combination of Gaussian function. The minimal STO-3G basis set approximates Slater orbitals (Slater Type Orbitals-STO) by including three Gaussian functions. A split valence basis set increases the number of basis functions per atom. The 6-311G basis set is a split valence set method. The core electrons are represented by a single contracted Gaussian consisting of six Gaussian functions. The '6-311' indicates that the valence orbitals are split into three shells where the contracted Gaussians are represented by three, one and one primitive Gaussians respectively. Further, the polarized basis set add d functions to carbon and f functions to transition metals and is represented by * asterisk sign. The presence of second asterisk sign indicates that p functions are added to H atoms. Double asterisk ** can also be represented as (d,p). To include orbital expansion for occupying a large region of space, diffuse functions represented by '+' sign, can also be added. Similarly, a double plus sign indicates that diffuse functions are also added to the H atom. [18]

In this study we have used 6-311G++(d,p) basis set for all the calculations.

2.6.3 Level of Theory:

The purpose of all the theories is to find the energy and to calculate all the other parameters of a given molecule.

In quantum chemistry, the calculation for energy of a system implies the solution of Schrodinger equation:

$$H \psi = E \psi \dots\dots\dots (2.2)$$

Where, H is the Hamiltonian operator and ψ is the wave function (as defined by quantum mechanics postulates). The operator H is the sum of kinetic and potential energies so it represents the total energy of the system.

2.6.3.1 Hartree Fock (HF)

Hartree Fock calculation solves the Schrodinger Equation in the simplest way possible. This method was formulated by Hartree [42] in 1928. In this method the Hamiltonian is taken as the sum of Kinetic Energy and Potential Energy of individual electrons and the interaction and repulsion between them. Then the wave function for the system is assumed as the product of individual electrons including the fact that wave function should be antisymmetric.

2.6.3.2 Density Functional Theory

Density functional theory (DFT) is a theory of electronic structure, based on the electron density distribution $\rho(r)$, instead of the many-electron wave function $\psi(r_1, r_2, r_3, \dots)$ and was proposed by Hohenberg and Kohn (HK) [43-45].

(a) B3LYP

The B3LYP functional is based on the exchange-energy functional developed by Axel Becke in 1983 [46,47], which was then modified by the introduction of the Lee, Yang, Parr (LYP) in 1988 as a correlation-energy functional [48]. These functionals use the exchange energy given by Hartree-Fock theory to substitute into the exchange-correlation functional developed by LYP.

(b) M06

Minnesota functional was designed in 2006 as an improvement to reproduce dispersion forces well. This suit of program contains four functionals that are M06-L, M06, M06-2 X and M06-HF, each one having a different contribution of HF exchange. The advantage of using M06-2x is for studying main group thermochemistry, kinetics, non-covalent interactions, and electronic excitation energies.

2.6.4 Energy Calculations

2.6.4.1 Stabilization Energy Calculation:

The stabilization energy of the complex was calculated as defined below. The stabilization energy (ΔE) of a complex is given by

$$\Delta E = E_{\text{complex}} - (E_1 + E_2) \dots \dots \dots (2.3)$$

Where, E_1 , E_2 and E_{complex} represent the energies for the monomers 1, 2 and complex formed by 1 and 2 respectively. If the value of ΔE is negative, the complex is more stable relative to the precursors. The stabilization energy of the complex corrected for zero point energy (ZPE) was also calculated.

2.6.4.2 Zero Point Energy (ZPE)

From the quantum mechanics theory, the molecular vibrations do not vanish in ground state, vacuum and at 0K as referred by calculations, and have $0.5 h\nu$ value known as the Zero point vibrational energy. The Zero point energy is given by: [18]

$$E_{\text{zpve}} = 1/2 \sum_{i=1}^n h\nu(i) \dots\dots\dots (2.4)$$

Where, E_{zpve} represents the sum of Zero point vibrational energy having n vibrational degrees of freedom.

2.6.4.3 Basis Set Superposition Error (BSSE)

The use of larger basis set for the energy calculations of the monomers and the complex, lowers the stabilization energy obtained for the complex because each monomer can overlap the basis function of the other. This error is referred as Basis set superimposition error (BSSE) and is corrected by increasing the basis set until the stabilization energy is stable.

Gaussian 09 program gives correction for the BSSE by using Counterpoise method where it assumes the monomers of the complex to be different fragment as proposed by Boys and Bernadi [49]. In this method, one calculates all quantities (energies of monomer E_1 , E_2 and the complex E_{complex}) in the same basis set spanned by the functions of the complex and the difference is obtained as follows.

$$\Delta E = E_{\text{complex}}(\text{B}) - \{E_1(\text{B}) + E_2(\text{B})\} \dots\dots\dots (2.5)$$

Where, $E_1(\text{B})$ = Energy of the monomer 1 using the basis set B

$E_2(\text{B})$ = Energy of the monomer 2 using the basis set B

$E_{\text{complex}}(\text{B})$ = Energy of the complex using the basis set B

Corrections of energies for ZPE and BSSE [48] simultaneously were not included as these values are known to overcorrect the stabilization values.

2.6.5 Atoms in Molecules (AIM)

Atoms in Molecule theory was proposed by Bader to analyse the electron density topology by using the wave function of the optimized geometry of the complex using the G09 package [50].

From the electron density plots obtained by AIM, one obtains bond critical points, charge density (ρ), Laplacian of charge density ($\nabla^2\rho$). The charge density, $\rho(\mathbf{r})$, is a physical quantity having a definite value at each point in space. In the density plot, where it is a maximum, a minimum, or a saddle point, the first derivative of the charge density is zero and this point is known as a critical point. The sign of its second derivative or curvature at this point determines whether a function is maximum or minimum. The topological properties are summarized in terms of the number and nature of its critical points. The rank of critical point, ω , is equal to the number of non-zero eigenvalues or non-zero curvature of ρ at the critical point. The signature denoted by σ , is the algebraic sum of the signs of the eigenvalues. The critical point (CP) is labelled by giving the values (ω, σ). For example, (3, +1) critical point means, three non-zero curvatures and two positive and one negative eigenvalues. A (3, -1) CP correspond to a bond between two atoms, a (3, +1) CP to a ring, a (3, +3) CP to a cage and a (3, -3) CP corresponds to a maximum. The numbers of critical points of all types, which can coexist in a system with a finite number of nuclei, are governed by the Poincare- Hopf relationship,

$$n - b + r - c = 1 \dots\dots\dots (2.6)$$

Where, 'n' is the number of nuclei, 'b' is the number of bond critical points, 'r' is the number of ring critical points and 'c' is the number of cage critical points.

Chapter 3

STUDY ON THE COMPLEX FORMATION OF PHENYLACETYLENE-D AND METHANOL

In this chapter we discuss our results on the study of the complexes between Phac-D and methanol. The experimental procedure and computational methods used in this work has already been discussed in Chapter 2.

Result and Discussion

3.1 Experimental

Fig 3.1 and Fig 3.2 shows the matrix isolation infrared spectra of Phac-D and Methanol trapped in N_2 . In Fig 3.1, the spectra spans the region $2800-2400\text{cm}^{-1}$ (grid A) and $900-700\text{cm}^{-1}$ (grid B), which corresponds to C-D stretching and C-D bending of Phac-D respectively. In Fig 3.2, the spectra spans the region $4000-3500\text{cm}^{-1}$, which corresponds to O-H stretching. Fig 3.1, trace 'a' shows the infrared spectra of matrix isolated Phac-D alone in 1:1000 ratio annealed at a temperature of 32K for 30min. and then brought back to 12K. Trace 'b', in the same figure, shows the as deposited spectra at 12K of Phac-D and Methanol at a ratio of 1:1. In the same figure, trace 'c' and 'd' shows the annealed spectra of Phac-D and Methanol at a ratio of 1:1 and 1:3 respectively. In Fig 3.1, the methanol alone spectra is not shown because there is no methanol features in this region. In Fig 3.1, the main features of Phac-D occurs at 2599.4 , 769.4 and 757.5cm^{-1} . When the matrix was annealed at 32K there were new features at 2593.7 , 2554.0 and 764.2cm^{-1} . In Fig 3.2, trace 'a' shows the infrared spectra of matrix isolated Methanol alone in 6:1000 ratio annealed at a temperature of 32K for 30min. and then brought back to 12K. Trace 'b', in the same

figure, shows the as deposited spectra at 12K of Phac-D and Methanol at a ratio of 1:3. In the same figure, trace 'c' and 'd' shows the annealed spectra of Phac-D and Methanol at a ratio of 1:3 and 3:3 respectively. In Fig 3.2, the Phac-D alone spectra is not shown because there is no Phac-D features in this region. In Fig 3.2, the main features of Methanol occurs at 3663.2 cm^{-1} . The feature at 3727.3 cm^{-1} in trace 'b' is due to H_2O which is an inevitable impurity in any matrix isolation experiments. When the matrix was annealed at 32K there was a new feature at 3591.1 cm^{-1} . When the concentration of methanol is increased this new feature also increases, indicating that this new feature is due to Phac-D and Methanol complex formation. The occurrence of these features even at lower concentrations indicates that this is a 1:1 complex.

Fig 3.3 and Fig 3.4 shows the matrix isolation infrared spectra of Phac-D and Methanol trapped in Ar. In Fig 3.3, the spectra spans the region $2800\text{-}2400\text{ cm}^{-1}$ (grid A) and $900\text{-}700\text{ cm}^{-1}$ (grid B), which corresponds to C-D stretching and C-D bending of Phac-D respectively. In Fig 3.4, the spectra spans the region $4000\text{-}3500\text{ cm}^{-1}$, which corresponds to O-H stretching. Fig 3.3, trace 'a' shows the infrared spectra of matrix isolated Phac-D alone in 3: 1000 ratio annealed at a temperature of 35K for 30min and then brought back to 12K. Trace 'b', in the same figure, shows the as deposited spectra at 12K of Phac-D and Methanol at a ratio of 3:3. In the same figure, trace 'c' and 'd' shows the annealed spectra of Phac-D and Methanol at a ratio of 3:3 and 3:6 respectively. In Fig 3.3, the methanol alone spectra is not shown because there is no methanol features in this region. In Fig 3.3, the main features of Phac-D occurs at 2607.7 and 757 cm^{-1} . When the matrix was annealed at 35K there were new features at 2592.8 , 2559.4 and 765 cm^{-1} . In Fig 3.4, trace 'a' shows the infrared spectra of matrix isolated Methanol alone in 3:1000 ratio annealed at a temperature of 35K for 30min. and then brought back to 12K. Trace 'b', in the same figure, shows the as deposited spectra at 12K of Phac-D and Methanol at a ratio of 3:3. In the same figure, trace 'c' and 'd' shows the annealed spectra of Phac-D and Methanol at a ratio of 3:3 and 3:6 respectively. In Fig 3.4, the Phac-D alone spectra is not shown because there is no Phac-D features in this region. In Fig 3.4, the main feature of Methanol occurs at 3666.2 cm^{-1} . The features at 3776.6 , 3756.7 and 3710.4 cm^{-1} in trace 'b' is due to H_2O . When the matrix was annealed at 35K there is a new feature at 3591.4 cm^{-1} . When the concentration of methanol is increased these new features also increases, indicating that these new features are due to Phac-D and Methanol complex formation. The occurrence of these features even at lower concentrations of indicates that this is a 1:1 complex.

3.2 Computations

Geometry optimization was performed at the B3LYP/6-311G++(d,p) and M062x/6-311G++(d,p). At B3LYP/6-311G++(d,p) level of theory, three minima for the complex between Phac-D and Methanol were obtained. The corresponding structures are shown in Fig. 3.5 at B3LYP/6-311G++(d,p) and in Fig 3.6 at M062x/6-311G++(d,p), together with the stabilization energy for each complex. From the calculations for stabilization energy, Complex 1 is the most stable and the energy barrier of Complex 1 with Complex 2 and 3 is 0.79 kcal/mol and 0.19 kcal/mol, respectively, after correcting for ZPE.

At M062x/6-311G++(d,p) level of theory, four minima for the complex between Phac-D and Methanol were obtained. The corresponding structures are shown in Fig. 3.5, together with the stabilization energy for each complex. The calculation for stabilization energy shows Complex 2 to be the most stable. The energy barrier between Complex 2 with Complex 1, 3 and 4 is 1.87, 0.2 and 0.14 kcal/mol, respectively, after correcting for ZPE. The energies of the various complexes have been corrected for zero point (ZPE) and basis set superposition (BSSE), and are given in Table 3.1. Selected structural parameters for Complex 1, Complex 2, Complex 3 and Complex 4 are given in Table 3.2, 3.3, 3.4 and 3.5, respectively.

3.3 Vibrational Assignment of Phac-D – Methanol adduct(s)

3.3.1 Experiments in N₂

3.3.1.1 Features of Phac-D sub molecule in the Phac-D – Methanol adduct(s)

Fig 3.1a shows the matrix isolation infrared spectra of Phac-D trapped in N₂. The spectral features at 2599.4 and 757.5cm⁻¹ are essentially due to C-D stretching and bending modes, which is also indicated by the computational calculations. The feature at 2601.1cm⁻¹ can be assigned to matrix site effect as this feature increased on annealing. The feature at 2577 and 769.4cm⁻¹ can be assigned to Phac-D – H₂O adduct, as water is always present in the matrix. When Phac-D was co-deposited with Methanol and the matrix then annealed, a strong feature was obtained at 2593.7 and 2554.0 cm⁻¹(Fig 3.1c and d, Grid A), which is red shifted by ~6cm⁻¹ and ~45cm⁻¹ from the C-D stretching monomer feature. The feature at 764.2cm⁻¹(Fig 3.1c and d, Grid B) is blue shifted by ~6cm⁻¹ from the C-D bending monomer feature. The vibrational frequencies together with their assignment are presented

in Table 3.6 and 3.7 at B3LYP/6-311G++(d,p) and in Table 3.8 and 3.9 at M062x/6-311G++(d,p) for C-D stretching and bending modes, respectively.

While the computations predict that there are three (B3LYP/6-311G++(d,p)) or four (M062x/6-311G++(d,p)) different adducts that can possibly be formed between the two precursors, with three or four different frequencies for the Phac-D submolecule, we observe only two clear features in the C-D stretching region and one clear feature at C-D bending region. The question of course is to identify which of the adducts are formed in the matrix. At the B3LYP/6-311G++(d,p) level, energy barrier of Complex 1 with Complex 2 and 3 is 0.79 kcal/mol and 0.19 kcal/mol, respectively, with Complex 1 being lower energy isomer. At M062x/6-311G++(d,p) level, the energy barrier between Complex 2 with Complex 1, 3 and 4 is 1.87, 0.2 and 0.14 kcal/mol, respectively, with Complex 2 being lower energy isomer. Therefore, by combining the two level of theories it is difficult to rule out any of the complex.

From frequency calculations, at B3LYP/6-311G++(d,p) level, scaled frequencies of complex 1, 2 and 3 show red shift in the stretch of Phac-D submolecule of 49 cm⁻¹, 0.2 cm⁻¹ and 7 cm⁻¹, while experimentally we observe a red shift of 45cm⁻¹ and 6cm⁻¹ (Table 3.6). At M062x/6-311G++(d,p) level, scaled frequencies of complex 1, 2, 3 and 4 show red shift in the stretch of Phac-D submolecule of 55 cm⁻¹, 4 cm⁻¹, 11 cm⁻¹ and 21 cm⁻¹, while experimentally we observe a red shift of 45cm⁻¹ and 6cm⁻¹ (Table 3.8). Therefore, there appears to be a better agreement of experimental and computed frequencies for Complex 1 and 3, which are the lowest energy conformers at B3LYP/6-311G++(d,p).

Frequency calculations, at B3LYP/6-311G++(d,p) level, scaled frequencies of complex 1, 2 and 3 show blue shift in the bend of Phac-D submolecule of 1 cm⁻¹, 2 cm⁻¹ and 1 cm⁻¹, while experimentally we observe a blue shift of 6 cm⁻¹ (Table 3.7). At M062x/6-311G++(d,p) level, scaled frequencies of complex 1, 2, 3 and 4 show red shift in the stretch of Phac-D submolecule of 10 cm⁻¹, 6 cm⁻¹, 10 cm⁻¹ and 6 cm⁻¹, while experimentally we observe a red shift of 7 cm⁻¹ (Table 3.9). Therefore, from the experimental and computed frequencies it is difficult to assign the conformer formed, but the appearance of this shift confirms the formation of the complex.

3.3.1.2 Features of Methanol submolecule in the Phac-D – Methanol adduct

Fig 3.2a shows the matrix isolation infrared spectra of Phac-D trapped in N₂. The spectral feature at 3663.3 cm⁻¹ is essentially due to O-H stretching modes, which is also indicated

by the computational calculations. The feature at 3727.3cm^{-1} can be assigned to H_2O . When Phac-D was co-deposited with Methanol and the matrix then annealed, a strong feature was obtained at 3591.4cm^{-1} (Fig 3.2c and d), which is red shifted by $\sim 72\text{cm}^{-1}$ from the O-H stretching monomer feature. The vibrational frequencies together with their assignment are presented in Table 3.10 at B3LYP/6-311G++(d,p) and in Table 3.11 at M062x/6-311G++(d,p).

From frequency calculations, at B3LYP/6-311G++(d,p) level, scaled frequencies of complex 1 show blue shift in the stretch of Methanol submolecule of 5cm^{-1} and Complex 2 and 3 show red shift of 24cm^{-1} and 64cm^{-1} , while experimentally we observe red shift of 72cm^{-1} (Table 3.10). At M062x/6-311G++(d,p) level, scaled frequencies of complex 1 show blue shift in the stretch of Methanol submolecule of 15cm^{-1} and Complex 2, 3 and 4 show red shift of 7cm^{-1} , 21cm^{-1} and 37cm^{-1} , while experimentally we observe a red shift of 72cm^{-1} (Table 3.11). Therefore, there appears to be a better agreement of experimental and computed frequencies for Complex 3 at B3LYP/6-311G++(d,p) level of theory.

3.3.2 Experiments in Argon

3.3.2.1 Features of Phac-D sub molecule in the Phac-D – Methanol adduct(s)

Fig 3.3a shows the matrix isolation infrared spectra of Phac-D trapped in Ar. The spectral features at 2607.7 and 757cm^{-1} are essentially due to C-D stretching and bending modes, which is also indicated by the computational calculations. The feature at 2597.8cm^{-1} can be assigned to matrix site effect as this feature increased on annealing. The feature at 2574cm^{-1} can be assigned to Phac-D – H_2O adduct. When Phac-D was co-deposited with Methanol and the matrix then annealed, a strong feature was obtained at 2593.7 and 2559.4cm^{-1} (Fig 3.3c and d, Grid A), which is red shifted by $\sim 14\text{cm}^{-1}$ and $\sim 49\text{cm}^{-1}$ from the C-D stretching monomer feature. The feature at 765cm^{-1} (Fig 3.3c and d, Grid B) is blue shifted by $\sim 8\text{cm}^{-1}$ from the C-D bending monomer feature. The vibrational frequencies together with their assignment are presented in Table 3.12 and 3.13 at B3LYP/6-311G++(d,p) and in Table 3.14 and 3.15 at M062x/6-311G++(d,p) for C-D stretching and bending modes, respectively.

From frequency calculations, at B3LYP/6-311G++(d,p) level, scaled frequencies of complex 1, 2 and 3 show red shift in the stretch of Phac-D submolecule of 49 cm⁻¹, 0.2 cm⁻¹ and 7 cm⁻¹, while experimentally we observe a red shift of 49cm⁻¹ and 15cm⁻¹ (Table 3.12). At M062x/6-311G++(d,p) level, scaled frequencies of complex 1, 2, 3 and 4 show red shift in the stretch of Phac-D submolecule of 55 cm⁻¹, 4 cm⁻¹, 12 cm⁻¹ and 20 cm⁻¹, while experimentally we observe a red shift of 49cm⁻¹ and 15cm⁻¹ (Table 3.13). Therefore, there appears to be a better agreement of experimental and computed frequencies for Complex 1 and 3, which are the lowest energy conformers at B3LYP/6-311G++(d,p).

Frequency calculations, at B3LYP/6-311G++(d,p) level, scaled frequencies of complex 1, 2 and 3 show blue shift in the bend of Phac-D submolecule of 1 cm⁻¹, 3 cm⁻¹ and 2 cm⁻¹, while experimentally we observe a blue shift of 8cm⁻¹ (Table 3.14). At M062x/6-311G++(d,p) level, scaled frequencies of complex 1, 2, 3 and 4 show red shift in the stretch of Phac-D submolecule of 0.6 cm⁻¹, 5 cm⁻¹, 1 cm⁻¹ and 6 cm⁻¹, while experimentally we observe a red shift of 8cm⁻¹ (Table 3.15). Therefore, from the experimental and computed frequencies it is difficult to assign the conformer formed, but the appearance of this shift confirms the formation of the complex.

3.3.2.2 Features of Methanol submolecule in the Phac-D – Methanol adduct

Fig 3.4a shows the matrix isolation infrared spectra of Phac-D trapped in Ar. The spectral feature at 3666.2 cm⁻¹ is essentially due to O-H stretching modes, which is also indicated by the computational calculations. The feature at 3776.6, 3756.7 and 3710.4 cm⁻¹ can be assigned to H₂O. When Phac-D was co-deposited with Methanol and the matrix then annealed, a strong feature was obtained at 3591.4 cm⁻¹(Fig 3.4c and d), which is red shifted by ~78 cm⁻¹ from the O-H stretching monomer feature. The vibrational frequencies together with their assignment are presented in Table 3.16 at B3LYP/6-311G++(d,p) and in Table 3.17 at M062x/6-311G++(d,p).

From frequency calculations, at B3LYP/6-311G++(d,p) level, scaled frequencies of complex 1, 2 and 3 show red shift in the stretch of Methanol submolecule of 2 cm⁻¹, 27 cm⁻¹ and 67 cm⁻¹, while experimentally we observe a red shift of 78 cm⁻¹ (Table 3.16). At M062x/6-311G++(d,p) level, scaled frequencies of complex 1 show a blue of 15cm⁻¹ and Complex 2, 3 and 4 show red shift in the stretch of Phac-D submolecule of 16 cm⁻¹, 30 cm⁻¹ and 40 cm⁻¹, while experimentally we observe a red shift of 72 cm⁻¹ (Table 3.17).

Therefore, there appears to be a better agreement of experimental and computed frequencies for Complex 3 at B3LYP/6-311G++(d,p).

3.4 Atoms in Molecules Study

An examination of the charge density topology was performed using the atoms-in molecules (AIM) theory of Bader. (3, -1) bond critical points (BCP) that could be associated with complexes 1, 2 and 3 and 4 were located as shown in Fig 3.7 at B3LYP/6-311G++(d,p) and in Fig 3.8 at M062x/6-311G++(d,p). The electron density ($\rho(r_c)$) and Laplacian of electron density $\nabla^2\rho(r_c)$ were computed for the critical points and the values are shown in Table 3.18 at B3LYP/6-311G++(d,p) and in Table 3.19 at M062x/6-311G++(d,p). The $\rho(r_c)$ and $\nabla^2\rho(r_c)$ values for bond critical points in both the complexes were found to be in the order of 10^{-2} au.

At B3LYP/6-311G++(d,p) level, in complex 3 a secondary interaction was also present between O of methanol and H of benzene ring in Phac-D. At M062x/6-311G++(d,p) level, in Complex 2 a secondary interaction was between methyl group of Methanol and C of benzene ring in Phac-D, in Complex 3 a secondary interaction was between O of methanol and H of benzene ring in Phac-D and, in complex 4, a secondary interaction was also present between benzene ring of Phac-D and methyl group of Methanol. The secondary interactions are mentioned as BCP2 in Table 3.18 at B3LYP/6-311G++(d,p) and in Table 3.19 at M062x/6-311G++(d,p).

3.5 Conclusions

The infrared spectra of Phac-D and Methanol trapped in solid N₂ and Ar, were studied. The experiments and computations clearly indicate the formation of Complex 1 and Complex 3. At B3LYP/6-311G++(d,p) level of theory indicates that the energy barrier between Complex 1 with Complex 2 and 3 is less and therefore, there is possibility for the three conformation to exist in the experiment. Frequency shifts calculation does not show any significant shift for Complex 2 but energy calculations does not rule out the possibility of its existence. Similarly, at M062x/6-311G++(d,p) level of theory the energy barrier between Complex 2 with Complex 1 and 3 is less and therefore, the other complexes might exist in the experiment but from frequency shift they were difficult to assign.

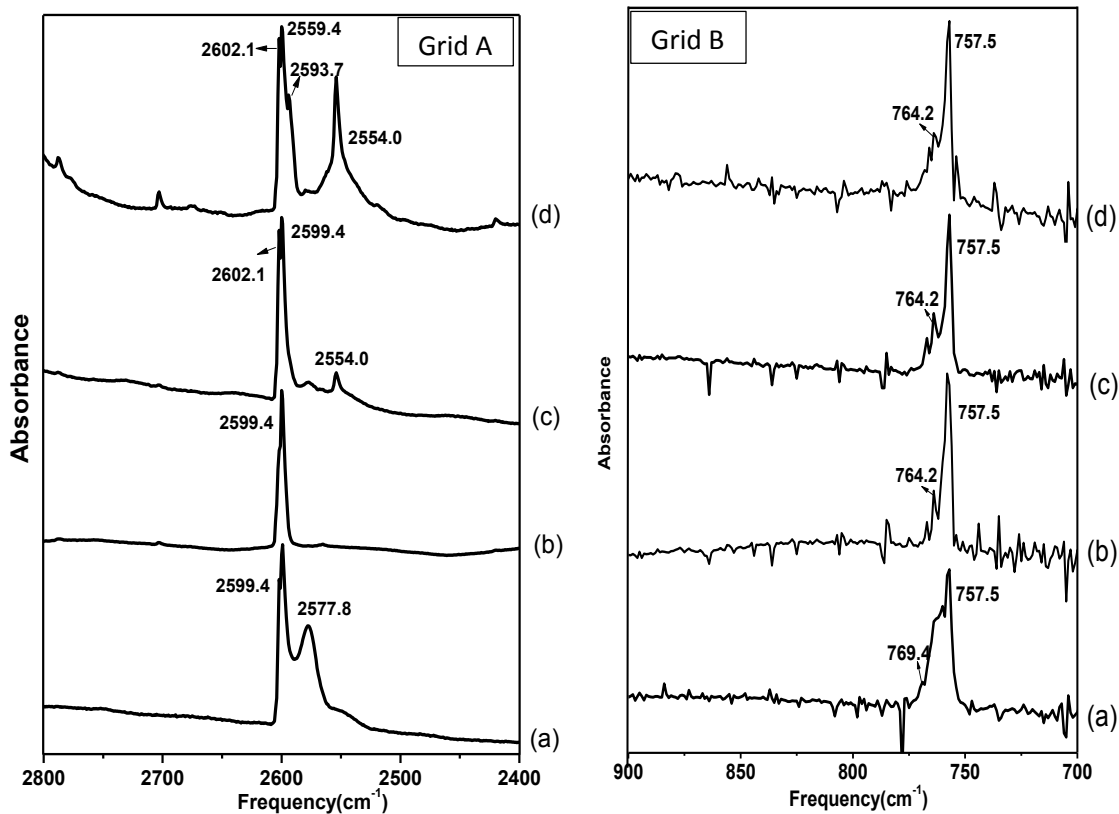


Fig 3.1: IR Spectra of Phac-D and Methanol in Nitrogen, the spectra spans the region from 2800-2400cm⁻¹ and 900-700cm⁻¹, (a) Phac-D alone (1:1000) annealed at 32K, (b) Phac-D : Methanol at 12K (1:1), (c) Phac-D: Methanol annealed at 32K and then brought back to 12K (1:1), (d) Phac-D: Methanol annealed at 32K and then brought back to 12K (1:3).

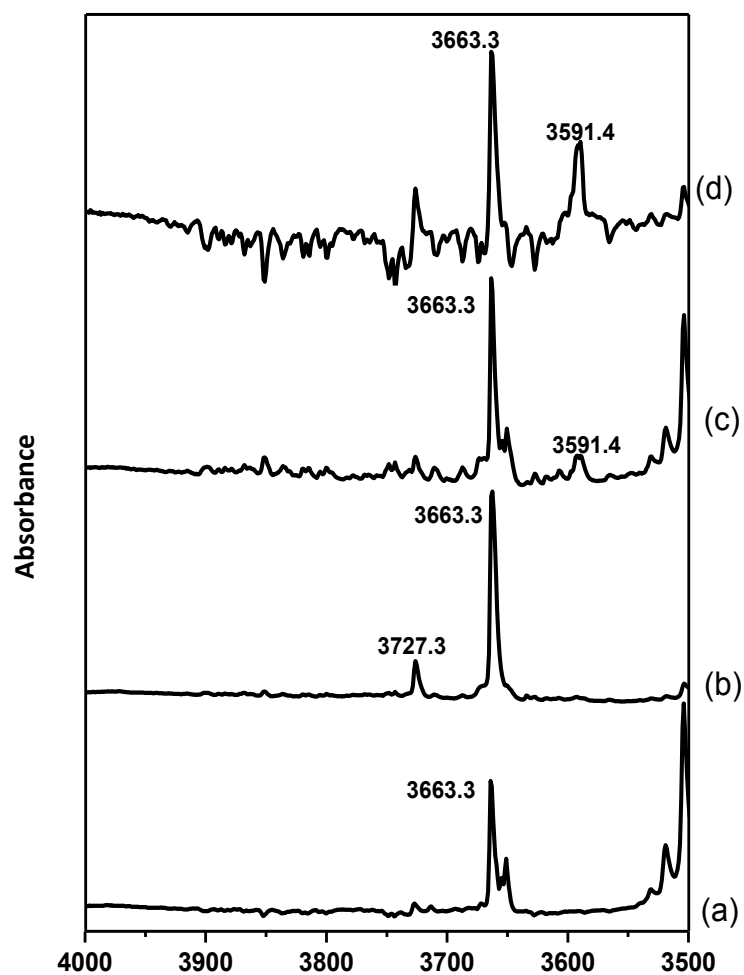


Fig 3.2: IR Spectra of Phac-D and Methanol in Nitrogen, the spectra spans the region from 4000-3500cm⁻¹, (a) Methanol alone (6:1000) annealed at 32K, (b) Phac-D : Methanol at 12K (1:3), (c) Phac-D: Methanol annealed at 32K and then brought back to 12K (1:3), (d) Phac-D: Methanol annealed at 32K and then brought back to 12K (3:3).

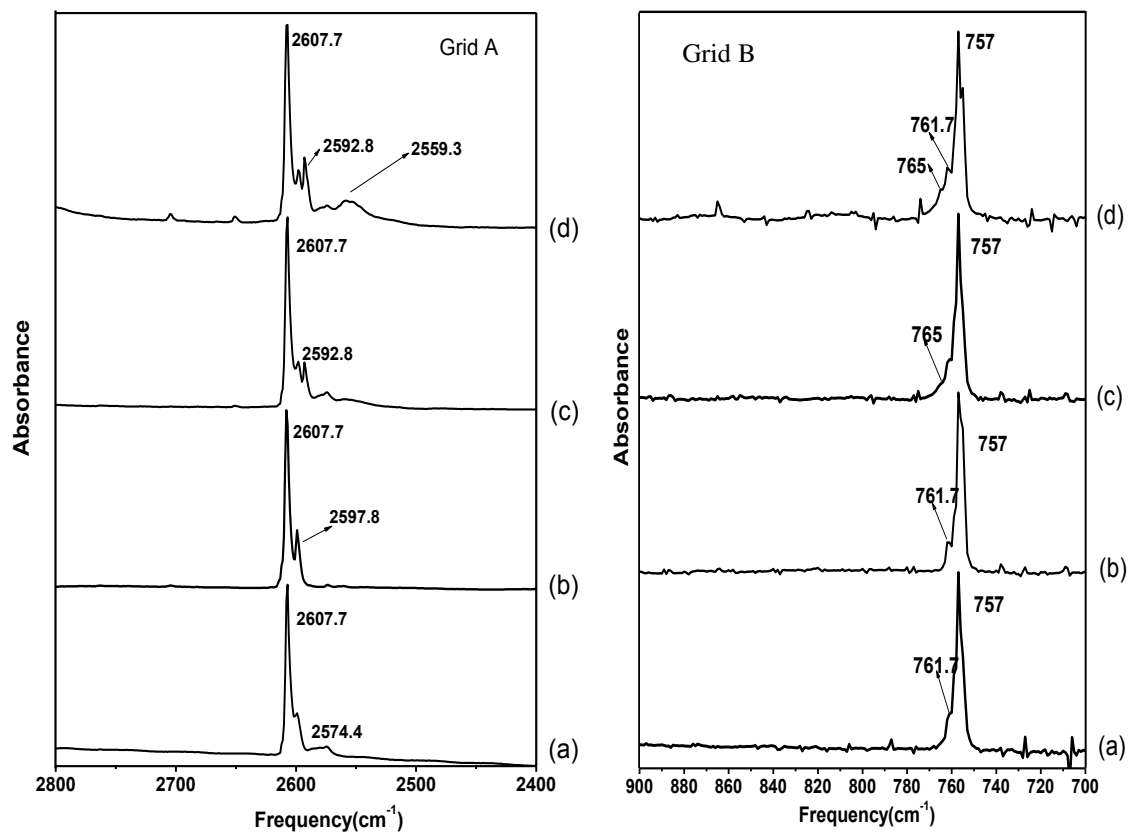


Fig 3.3: IR Spectra of Phac-D and Methanol in Argon, the spectra spans the region from 2800-2400cm⁻¹ and 900-700cm⁻¹, (a) Phac-D alone (3:1000) annealed at 35K and recorded at 12K, (b) Phac-D : Methanol at 12K (1:1), (c) Phac-D: Methanol annealed at 35K and then brought back to 12K (3:3), (d) Phac-D: Methanol annealed at 35K and then brought back to 12K (3:6).

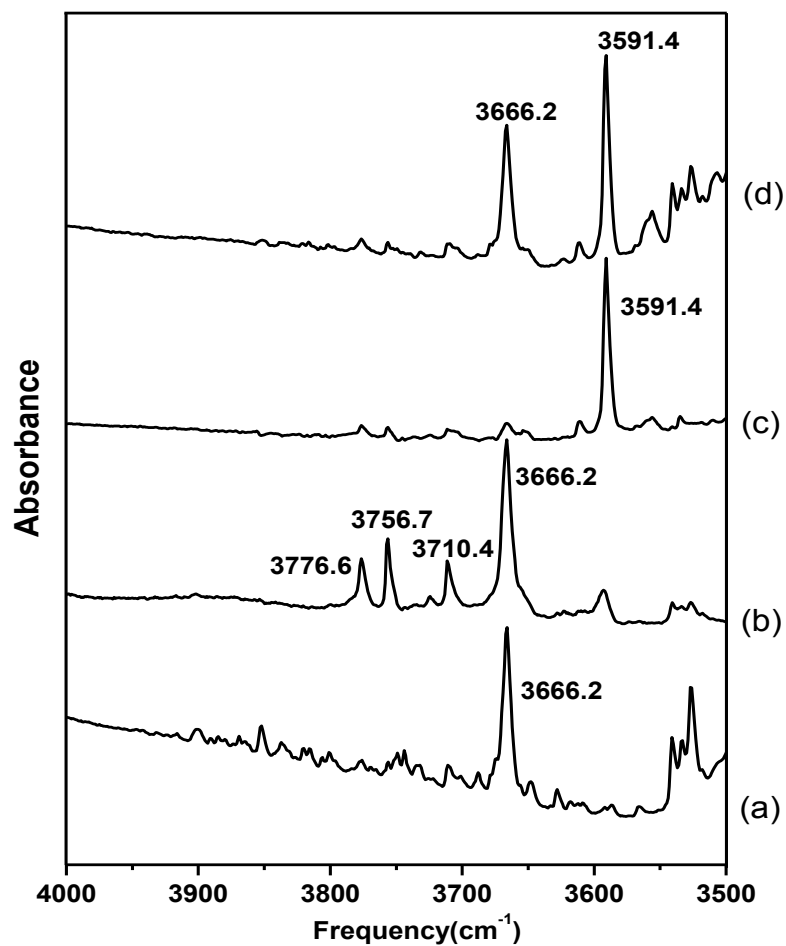
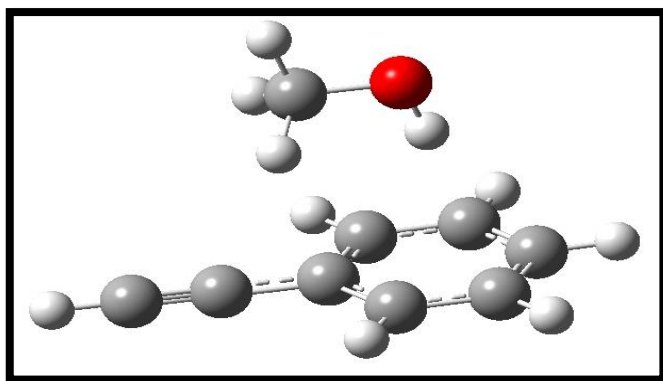


Fig 3.4: IR Spectra of Phac-D and Methanol in Nitrogen, the spectra spans the region from 4000-3500cm⁻¹, (a) Methanol alone (3:1000) annealed at 35K and recorded at 12K, (b) Phac-D : Methanol at 12K (3:3), (c) Phac-D: Methanol annealed at 35K and then brought back to 12K (3:3), (d) Phac-D: Methanol annealed at 35K and then brought back to 12K (3:6).

**TABLE 3.1: Stabilization Energy for Phac-D and Methanol Complexes
(Raw/ZP/BSSE) in kcal mol⁻¹**

Structures of Phac-D and Methanol	B3LYP/6-311G++(d,p)	M062x/6-311G++(d,p)
Complex1	-3.05/-2.02/-2.50	-4.01/-3.01/-3.55
Complex2	-1.74/-1.23/-1.28	-5.60/-4.88/-4.82
Complex3	-2.71/-1.83/-2.35	-5.63/-4.68/-5.06
Complex4	-----	-5.57/-4.74/-4.76

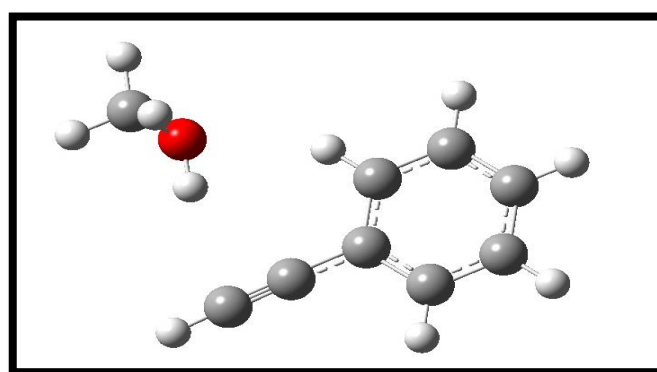


Raw	ZP	BSSE
-1.74	-1.23	-1.28

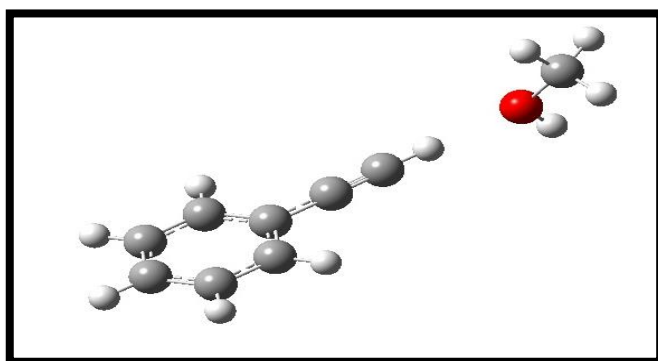
Complex2

*Stabilization Energy
In kcal mol⁻¹*

Raw	ZP	BSSE
-2.71	-1.83	-2.35



Complex3

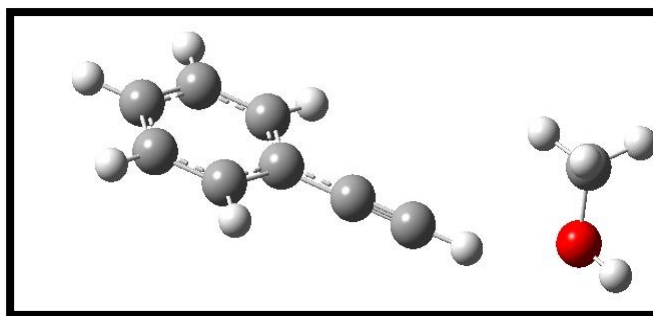


Raw	ZP	BSSE
-3.05	-2.02	-2.50

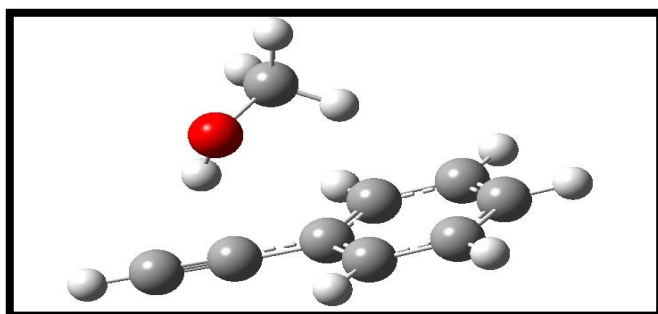
Complex1

Fig 3.5: Complex structure between Phac-D and Methanol at B3LYP/6-311G++(d,p) with stabilization energy

Raw	ZP	BSSE
-4.01	-3.01	-3.55



Complex1



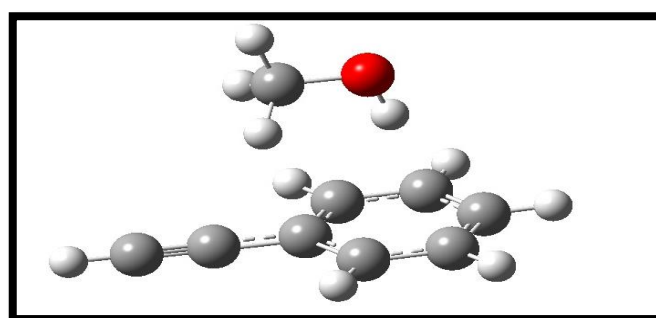
Complex4

Raw	ZP	BSSE
-5.57	-4.74	-4.76

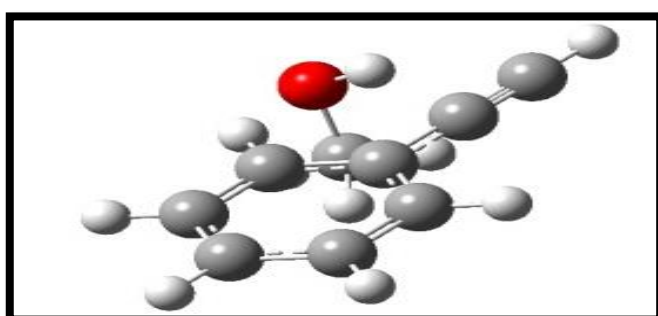
Stabilization Energy

In kcal mol⁻¹

Raw	ZP	BSSE
-5.60	-4.88	-4.82



Complex2



Complex3

Raw	ZP	BSSE
-5.63	-4.68	-5.06

Fig 3.6: Complex structure between Phac-D and Methanol at M062x/6-311G++(d,p) with stabilization energy

Table 3.2: Some selected geometrical parameters of Complex 1 at B3LYP/6-311G++(d,p) and M062x/6-311G++(d,p) where bond length is given in Å , bond angle in degree(°) and torsional angles in degree(°)

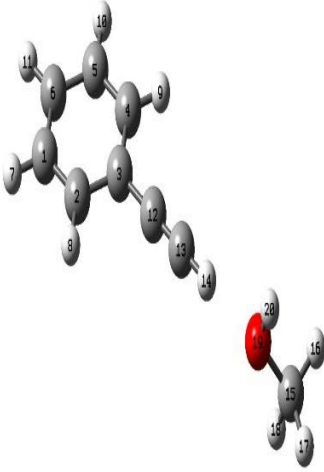
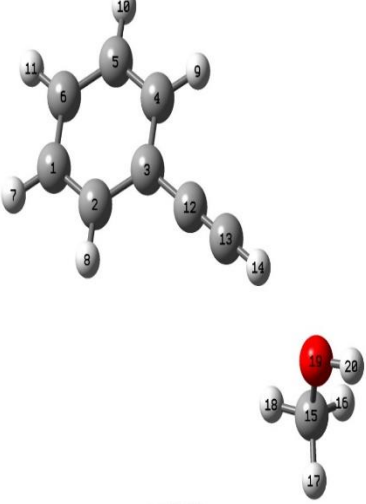
Complex 1	B3LYP/6-311G++(d,p)	M062x/6-311G++(d,p)
		
D14-O19	2.16	2.11
D14-C13	1.07	1.07
H20-O19-D14	119.5	139.0
C15-O19-D14	122.1	103.4
C13-D14-O19	178.9	154.7
C13-D14-O19-H20	97.7	147.6
C13-D14-O19-C15	-45.4	4.5

Table 3.3: Some selected geometrical parameters of Complex 2 at B3LYP/6-311G++(d,p) and M062x/6-311G++(d,p) where bond length is given in Å , bond angle in degree(°) and torsional angles in degree(°)

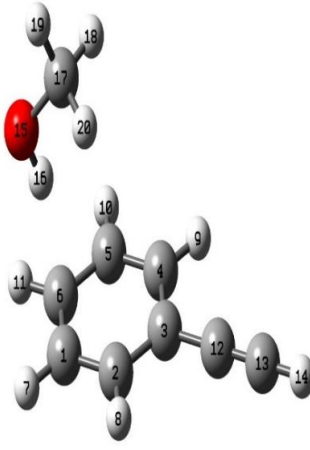
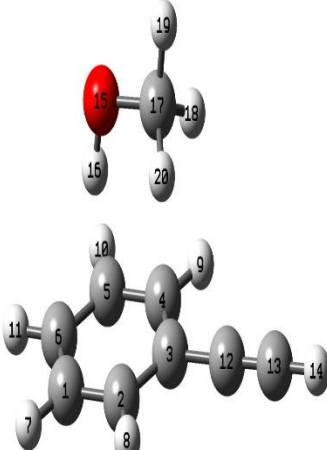
Complex 2	B3LYP/6-311G++(d,p)	M062x/6-311G++(d,p)
		
C1-H16	2.65	2.68
C6-H16	2.72	2.66
C5-H16	3.31	2.70
O15-H16-C1	156.9	156.9
O15-H16-C6	157.3	167.7
O15-H16-C5	154.6	149.6
H16-C6-H11	95.2	118.2
O15-H16-C6-H11	-9.2	-18.1
O15-H16-C6-C1	-129.1	-134.8
O15-H16-C6-C5	113.3	99.0

Table 3.4: Some selected geometrical parameters of Complex 3 at B3LYP/6-311G++(d,p) and M062x/6-311G++(d,p) where bond length is given in Å , bond angle in degree(°) and torsional angles in degree(°)

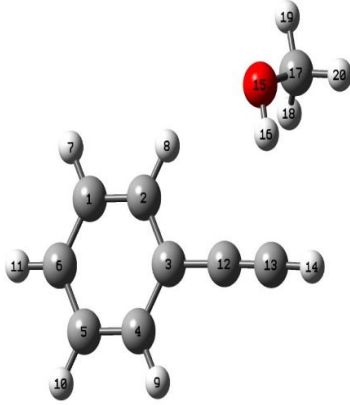
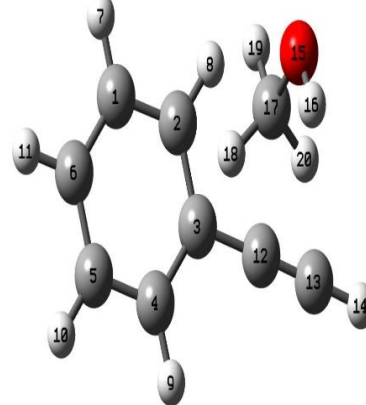
Complex 3	B3LYP/6-311G++(d,p)	M062x/6-311G++(d,p)
		
C12-H16	2.57	2.50
C13-H16	2.49	2.50
O15-H8	2.5	2.42
O15-H16-C12	145.7	135.1
O15-H16-C13	173.2	153.9
H16-O15-H8	76.3	77.3
O15-H16-C12-C3	1.4	-34.4
O15-H16-C13-D14	-172.5	114.1
H16-O15-H8-C2	-19.5	-59.3

Table 3.5: Some selected geometrical parameters of Complex 4 at M062x/6-311G++(d,p) where bond length is given in Å , bond angle in degree(°) and torsional angles in degree(°)

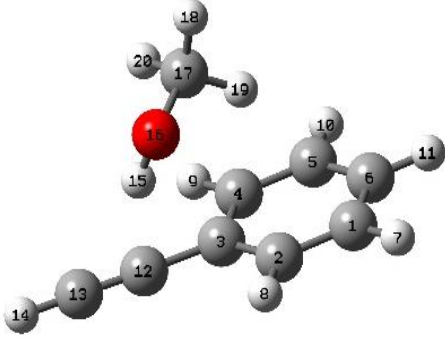
Complex 4	M062x/6-311G++(d,p)
	
C12-H15	2.42
C13-H15	2.71
C2-H19	2.84
C3-H19	2.84
C4-H19	3.00
C17-H19-C2	119.7
C17-H19-C3	107.0
C17-H19-C4	116.6
O16-H15-C12	153.3
O16-H15-C13	172.0
H15-O16-C17-H19	-74.2
O16-H15-C13-D14	-84.8
O16-H15-C12-C3	18.0
C17-H19-C3-C12	-4.5

Table 3.6: Calculated and experimental frequency table for shifts (cm⁻¹) in Phenylacetylene-D (Phac-D) C-D stretching due to the formation of Phenylacetylene-D and Methanol complexes in N₂ matrix at B3LYP/6-311G++(d,p)

<u>Nitrogen</u>	<u>Unscaled Freq.</u>	<u>Scaled Freq.</u>	<u>Scaling Factor</u>	<u>Exptl. Freq.</u>	<u>Δv (exp-scaled)</u>	<u>Mode of assignment</u>
<u>Phac-D</u>	2711.7	2599.4		2599.4		C-D stretching
<u>Complex1</u>	2660.9	2550.7	0.9586	2554.0	3.3	C-D stretching
<u>Complex2</u>	2711.9	2599.6	0.9586			C-D stretching
<u>Complex3</u>	2704.6	2592.6	0.9586	2593.7	1.1	C-D stretching

Table 3.7: Calculated and experimental frequency table for shifts (cm⁻¹) in Phenylacetylene-D (Phac-D) C-D bending due to the formation of Phenylacetylene-D and Methanol complexes in N₂ matrix at B3LYP/6-311G++(d,p)

<u>Nitrogen</u>	<u>Unscaled Freq.</u>	<u>Scaled Freq.</u>	<u>Scaling Factor</u>	<u>Exptl. Freq.</u>	<u>Δv (exp-scaled)</u>	<u>Mode of assignment</u>
<u>Phac-D</u>	773.3	757.5		757.5		C-D bending
<u>Complex1</u>	774.4	758.1	0.9789	764.0	5.9	C-D bending
<u>Complex2</u>	777.1	760.0	0.9789	764.0	4.0	C-D bending
<u>Complex3</u>	775.4	759.0	0.9789	764.0	5.0	C-D bending

Table 3.8: Calculated and experimental frequency table for shifts (cm⁻¹) in Phenylacetylene-D (Phac-D) C-D stretching due to the formation of Phenylacetylene-D and Methanol complexes in N₂ matrix at M062x/6-311G++(d,p)

<u>Nitrogen</u>	<u>Unscaled Freq.</u>	<u>Scaled Freq.</u>	<u>Scaling Factor</u>	<u>Exptl. Freq.</u>	<u>Δv (exp-scaled)</u>	<u>Mode of assignment</u>
<u>Phac-D</u>	2740			2599.4		C-D stretching
<u>Complex1</u>	2682.4	2544.5	0.9486	2554.0	9.5	C-D stretching
<u>Complex2</u>	2736	2595.4	0.9486			C-D stretching
<u>Complex3</u>	2727.9	2587.7	0.9486	2593.7	6	C-D stretching
<u>Complex4</u>	2719.5	2579.7	0.9486	2593.7	14	C-D stretching

Table 3.9: Calculated and experimental frequency table for shifts (cm⁻¹) in Phenylacetylene-D (Phac-D) C-D bending due to the formation of Phenylacetylene-D and Methanol complexes in N₂ matrix at M062x/6-311G++(d,p)

<u>Nitrogen</u>	<u>Unscaled Freq.</u>	<u>Scaled Freq.</u>	<u>Scaling Factor</u>	<u>Exptl. Freq.</u>	<u>Δv (exp-scaled)</u>	<u>Mode of assignment</u>
<u>Phac-D</u>	773.3	757.5		757.5		C-D bending
<u>Complex1</u>	783.7	767.9	0.9798	764.0		C-D bending
<u>Complex2</u>	779.6	763.9	0.9798	764.0		C-D bending
<u>Complex3</u>	783.1	767.3	0.9797	764.0		C-D bending
<u>Complex4</u>	779.1	763.4	0.9798	764.0		C-D bending

Table 3.10: Calculated and experimental frequency table for shifts (cm⁻¹) in Methanol O-H stretching frequency due to the formation of Phenylacetylene-D and Methanol complexes in N₂ matrix at B3LYP/6-311G++(d,p)

<u>Nitrogen</u>	<u>Unscaled Freq.</u>	<u>Scaled Freq.</u>	<u>Scaling Factor</u>	<u>Exptl. Freq.</u>	<u>Δv (exp-scaled)</u>	<u>Mode of assignment</u>
<u>Methanol</u>	3845.5	3663.3		3663.3		O-H stretching
<u>Complex1</u>	3861.2	3668.1	0.95			O-H stretching
<u>Complex2</u>	3830.9	3639.4	0.95			O-H stretching
<u>Complex3</u>	3789.2	3599.7	0.95	3591.4	-8.3	O-H stretching

Table 3.11: Calculated and experimental frequency table for shifts (cm⁻¹) in Methanol O-H stretching frequency due to the formation of Phenylacetylene-D and Methanol complexes in Argon matrix at M062x/6-311G++(d,p)

<u>Nitrogen</u>	<u>Unscaled Freq.</u>	<u>Scaled Freq.</u>	<u>Scaling Factor</u>	<u>Exptl. Freq.</u>	<u>Δv (exp-scaled)</u>	<u>Mode of assignment</u>
<u>Methanol</u>	3932.9	3663.3		3663.3		O-H stretching
<u>Complex1</u>	3948.6	3678.1	0.9315			O-H stretching
<u>Complex2</u>	3924.9	3656.1	0.9315			O-H stretching
<u>Complex3</u>	3910	3642.2	0.9315			O-H stretching
<u>Complex4</u>	3899.5	3626.5	0.9315	3591.4	-35.1	O-H stretching

Table 3.12: Calculated and experimental frequency table for shifts (cm⁻¹) in Phenylacetylene-D (Phac-D) C-D stretching due to the formation of Phenylacetylene-D and Methanol complexes in Argon matrix at B3LYP/6-311G++(d,p)

<u>Argon</u>	<u>Unscaled Freq.</u>	<u>Scaled Freq.</u>	<u>Scaling Factor</u>	<u>Exptl. Freq.</u>	<u>Δv (exp-scaled)</u>	<u>Mode of assignment</u>
<u>Phac-D</u>	2711.7	2607.7		2607.7		C-D stretching
<u>Complex1</u>	2660.9	2558.7	0.9616	2559.3	0.6	C-D stretching
<u>Complex2</u>	2711.9	2607.8	0.9616			C-D stretching
<u>Complex3</u>	2704.6	2600.7	0.9616	2592.8	-7.9	C-D stretching

Table 3.13: Calculated and experimental frequency table for shifts (cm⁻¹) in Phenylacetylene-D (Phac-D) C-D bending due to the formation of Phenylacetylene-D and Methanol complexes in Argon matrix at B3LYP/6-311G++(d,p)

<u>Argon</u>	<u>Unscaled Freq.</u>	<u>Scaled Freq.</u>	<u>Scaling Factor</u>	<u>Exptl. Freq.</u>	<u>Δv (exp-scaled)</u>	<u>Mode of assignment</u>
<u>Phac-D</u>	773.3	757.0		757.0		C-D bending
<u>Complex1</u>	774.4	758.1	0.9789	765	7.1	C-D bending
<u>Complex2</u>	777.1	760.0	0.9789	765	5.2	C-D bending
<u>Complex3</u>	775.4	759.0	0.9789	765	6.2	C-D bending

Table 3.14: Calculated and experimental frequency table for shifts (cm⁻¹) in Phenylacetylene-D (Phac-D) C-D stretching due to the formation of Phenylacetylene-D and Methanol complexes in Argon matrix at M062x/6-311G++(d,p)

<u>Argon</u>	<u>Unscaled Freq.</u>	<u>Scaled Freq.</u>	<u>Scaling Factor</u>	<u>Exptl. Freq.</u>	<u>Δv (exp-scaled)</u>	<u>Mode of assignment</u>
<u>Phac-D</u>	2740	2607.7		2607.7		C-D stretching
<u>Complex1</u>	2682.4	2552.8	0.9517	2559.3	6.5	C-D stretching
<u>Complex2</u>	2736	2603.9	0.9517			C-D stretching
<u>Complex3</u>	2727.9	2596.1	0.9517	2592.8	3.3	C-D stretching
<u>Complex4</u>	2719.5	2588.1	0.9517	2592.8	4.7	C-D stretching

Table 3.15: Calculated and experimental frequency table for shifts (cm⁻¹) in Phenylacetylene-D (Phac-D) C-D bending due to the formation of Phenylacetylene-D and Methanol complexes in Argon matrix at M062x/6-311G++(d,p)

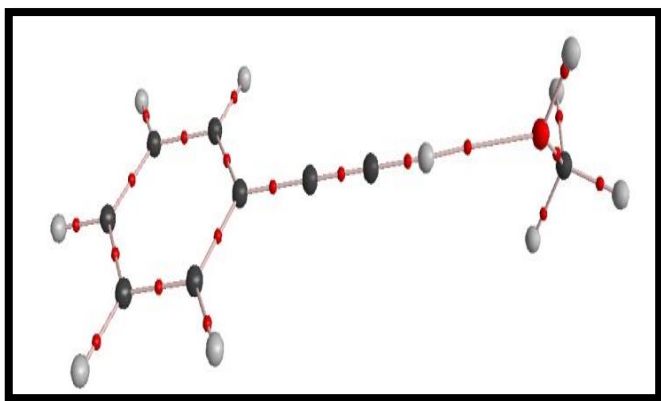
<u>Argon</u>	<u>Unscaled Freq.</u>	<u>Scaled Freq.</u>	<u>Scaling Factor</u>	<u>Exptl. Freq.</u>	<u>Δv (exp-scaled)</u>	<u>Mode of assignment</u>
<u>Phac-D</u>	784.3	757		757.0		C-D bending
<u>Complex1</u>	783.7	756.4	0.9652	765		C-D bending
<u>Complex2</u>	779.6	752.5	0.9652	765		C-D bending
<u>Complex3</u>	783.1	755.8	0.9652	765		C-D bending
<u>Complex4</u>	779.1	752.0	0.9652	765		C-D bending

Table 3.16: Calculated and experimental frequency table for shifts (cm⁻¹) in Methanol O-H stretching frequency due to the formation of Phenylacetylene-D and Methanol complexes in Argon matrix at M062x/6-311G++(d,p)

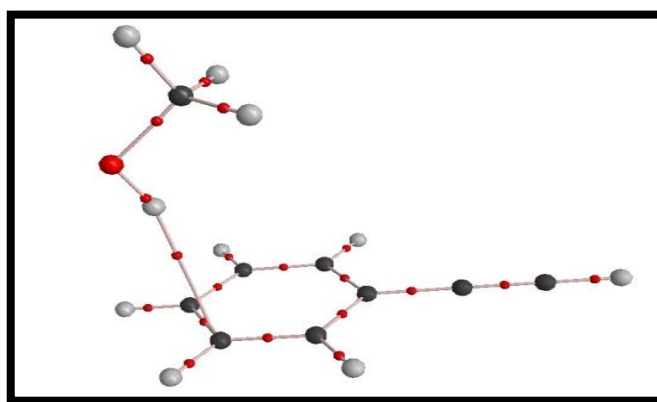
<u>Argon</u>	<u>Unscaled Freq.</u>	<u>Scaled Freq.</u>	<u>Scaling Factor</u>	<u>Exptl. Freq.</u>	<u>Δv (exp-scaled)</u>	<u>Mode of assignment</u>
<u>Methanol</u>	3845.5	3666.2		3666.2		O-H stretching
<u>Complex</u>	3861.2	3668.1	0.95			O-H stretching
<u>Complex2</u>	3830.9	3639.4	0.95			O-H stretching
<u>Complex3</u>	3789.2	3599.7	0.95	3591.4	8.3	O-H stretching

Table 3.17: Calculated and experimental frequency table for shifts (cm⁻¹) in Methanol O-H stretching frequency due to the formation of Phenylacetylene-D and Methanol complexes in Argon matrix at M062x/6-311G++(d,p)

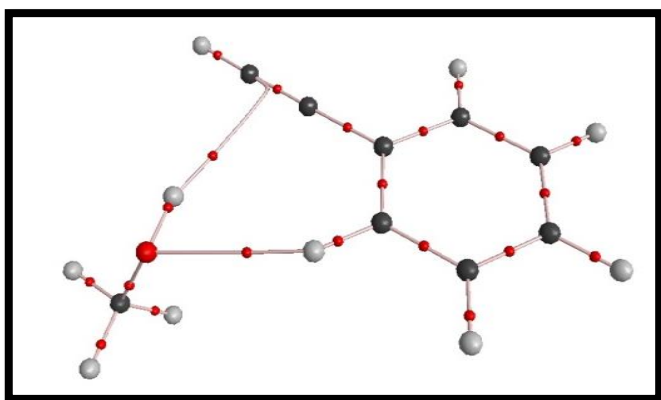
<u>Argon</u>	<u>Unscaled Freq.</u>	<u>Scaled Freq.</u>	<u>Scaling Factor</u>	<u>Exptl. Freq.</u>	<u>Δv (exp-scaled)</u>	<u>Mode of assignment</u>
<u>Methanol</u>	3932.9	3666.2		3666.2		O-H stretching
<u>Complex1</u>	3948.6	3680.9	0.93			O-H stretching
<u>Complex2</u>	3924.9	3650.2	0.93			O-H stretching
<u>Complex3</u>	3910	3636.3	0.9322			O-H stretching
<u>Complex4</u>	3899.5	3626.5	0.93	3591.4	-35.1	O-H stretching



Complex1

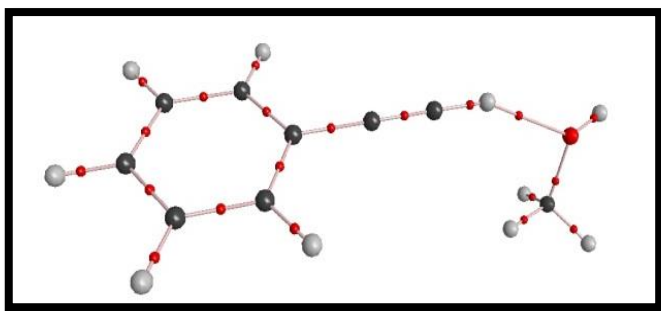


Complex2

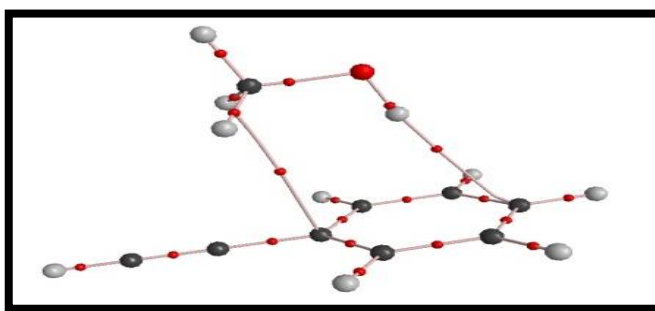


Complex3

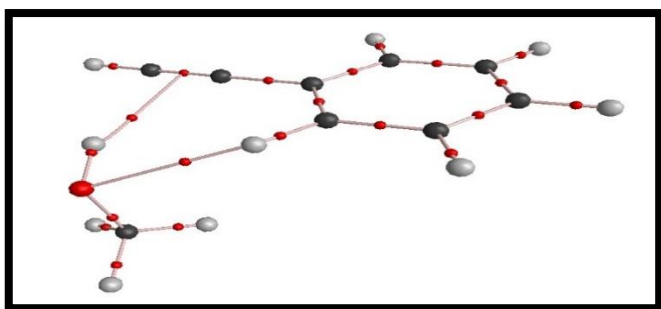
Fig 3.7: AIM analysis at B3LYP/6-311G++(d,p) level



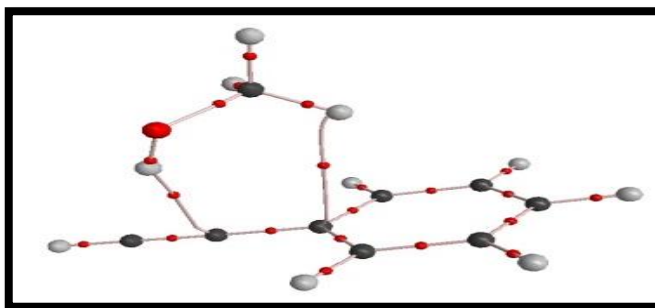
Complex1



Complex2



Complex3



Complex4

Fig 3.8: AIM analysis at M062x/6-311G++(d,p) level

Table 3.18 – Properties of different critical points present in Phac-D and Methanol complexes as a result of AIM analysis in B3LYP/6-311G++(d,p)

Complex	Critical Point	$\rho(\mathbf{rc})$	$\nabla^2\rho(\mathbf{rc})$
Complex 1	BCP	0.28486	0.25902
Complex 2	BCP	0.00741	-0.00501
Complex 3	BCP1	0.01074	-0.00775
	BCP2	0.00905	-0.00686

Table 3.19 – Properties of different critical points present in Phac-D and Methanol complexes as a result of AIM analysis in M062x/6-311G++(d,p).

Complex	Critical Point	$\rho(\mathbf{rc})$	$\nabla^2\rho(\mathbf{rc})$
Complex 1	BCP	0.01715	-0.01659
Complex 2	BCP1	0.00723	-0.00601
	BCP2	0.00625	-0.00553
Complex 3	BCP1	0.01343	-0.01075
	BCP2	0.01130	-0.00910
Complex 4	BCP1	0.01059	-0.00829
	BCP2	0.00738	-0.00608

Chapter 4

STUDY ON THE COMPLEX FORMATION OF PHENYLACETYLENE-D AND METHYLAMINE

In this chapter we discuss our results on the study of the complexes between Phac-D and methanol. The experimental procedure and computational methods used in this work has been discussed in Chapter 2.

Result and Discussion

4.1 Experimental

Fig 4.1 and Fig 4.2 shows the matrix isolation infrared spectra of Phac-D and Methylamine trapped in N_2 . In Fig 4.1, the spectra spans the region $2800-2400\text{cm}^{-1}$ (grid A) and $2000-1800\text{cm}^{-1}$ (grid B), which corresponds to C-D stretching and $C\equiv C$ stretching of Phac-D respectively. In Fig 4.2, the spectra spans the region $900-700\text{cm}^{-1}$, which corresponds to N-H bending and Phac-D bending. In Fig 4.1, trace 'a' shows the infrared spectra of matrix isolated Phac-D alone in 1:1000 ratio annealed at a temperature of 32K for 30min. and then brought back to 12K. Trace 'b', in the same figure, shows the as deposited spectra at 12K of Phac-D and Methylamine at a ratio of 1:1. In the same figure, trace 'c' and 'd' shows the annealed spectra of Phac-D and Methylamine at a ratio of 1:1 and 3:1 respectively. In Fig 4.1, the methylamine alone spectra is not shown because there is no methylamine feature in this region. In Fig 4.1, the main features of Phac-D occurs at 2599.4 cm^{-1} . When the matrix was annealed at 32K there were new features at 2523.0 , 1961 and 1941 cm^{-1} . In Fig 4.2, trace 'a' and 'b' shows the infrared spectra of matrix isolated Phac-D alone and Methylamine alone in 1:1000 ratio annealed at a temperature of 32K for 30min. and then

brought back to 12K, respectively. Trace 'c', in the same figure, shows the as deposited spectra at 12K of Phac-D and Methylamine at a ratio of 1:1. In the same figure, trace 'd' shows the annealed spectra of Phac-D and Methylamine at a ratio of 1:1. In Fig 4.2, the main features of Phac-D occurs at 757.5 cm^{-1} and of Methylamine at 816 cm^{-1} . When the matrix was annealed at 35K there were new features at 764 cm^{-1} and 843 cm^{-1} . When the concentration of methylamine was increased these new features also increases, indicating that these new features are due to Phac-D and Methylamine complex formation. The occurrence of these features even at lower concentrations of 1:1 indicates that this is a 1:1 complex.

Fig 4.3 and Fig 4.4 shows the matrix isolation infrared spectra of Phac-D and Methylamine trapped in Ar. In Fig 4.3, the spectra spans the region $2800\text{-}2500\text{ cm}^{-1}$ (grid A) and $2000\text{-}1800\text{ cm}^{-1}$ (grid B), which corresponds to C-D stretching and $\text{C}\equiv\text{C}$ stretching of Phac-D respectively. In Fig 4.4, the spectra spans the region $900\text{-}700\text{ cm}^{-1}$, which corresponds to N-H bending and Phac-D bending. Fig 4.1, trace 'a' shows the infrared spectra of matrix isolated Phac-D alone in 3:1000 ratio annealed at a temperature of 35K for 30 min. and then brought back to 12K. Trace 'b', in the same figure, shows the as deposited spectra at 12K of Phac-D and Methylamine at a ratio of 3:1.2. In the same figure, trace 'c' and 'd' shows the annealed spectra of Phac-D and Methylamine at a ratio of 3:1.2 and 3:1.4 respectively. In Fig 4.3, the methylamine alone spectra is not shown because there is no methylamine feature in this region. In Fig 4.3, the main features of Phac-D occurs at 2607.7 cm^{-1} . When the matrix was annealed at 35K there were new features at 2523.3 , 1961 and 1940 cm^{-1} . In Fig 4.4, trace 'a' and 'b' shows the infrared spectra of matrix isolated Phac-D alone and Methylamine alone in 3:1000 and 1.2:1000 ratio respectively, annealed at a temperature of 35K for 30min. and then brought back to 12K, respectively. Trace 'c', in the same figure, shows the as deposited spectra at 12K of Phac-D and Methylamine at a ratio of 3:1.2. In the same figure, trace 'd' shows the annealed spectra of Phac-D and Methylamine at a ratio of 3:1.2. In Fig 4.4, the main features of Phac-D occurs at 757 cm^{-1} and of Methylamine at 796.5 cm^{-1} . When the matrix was annealed at 35K there were new features at 765.7 and 810.5 cm^{-1} . When the concentration of methylamine was increased these new features also increases, indicating that these new features are due to Phac-D and Methylamine complex formation. The occurrence of these features even at lower concentrations of indicates that this is a 1:1 complex.

4.2 Computations

Geometry optimization was performed at the B3LYP/6-311G++(d,p) and M062x/6-311G++(d,p). At these level of theory, three minima for the complex between Phac-D and Methylamine were obtained. The corresponding structures are shown in Fig. 4.5 at B3LYP/6-311G++(d,p) and in Fig 4.6 at M062x/6-311G++(d,p), together with the stabilization energy for each complex. At the B3LYP/6-311G++(d,p) level of theory, from the calculations for stabilization energy, Complex 1 is the most stable and the energy barrier of Complex 1 with Complex 2 and 3 is 1.24 kcal/mol and 2.07 kcal/mol, respectively, after correcting for ZPE.

At M062x/6-311G++(d,p) level of theory, three minima for the complex between Phac-D and Methanol were obtained. The corresponding structures are shown in Fig. 4.7, together with the stabilization energy for each complex. The calculation for stabilization energy shows Complex 3 to be the most stable. The energy barrier between Complex 3 with Complex 1 and 2 is 0.0 and 0.2 kcal/mol, respectively, after correcting for ZPE. The energies of the various complexes have been corrected for zero point (ZPE) and basis set superposition (BSSE), and are given in Table 4.1. Selected structural parameters for Complex 1, Complex 2, and Complex 3 are given in Table 4.2, 4.3, and 4.4, respectively.

4.3 Vibrational Assignment

4.3.1 Experiments in N₂

4.3.1.1 Features of Phac-D submolecule in the Phac-D – Methylamine adduct(s)

Fig 4.1a shows the matrix isolation infrared spectra of Phac-D trapped in N₂. The spectral features at 2599.4 cm⁻¹ is essentially due to C-D stretching mode, which is also indicated by the computational calculation. The feature at 2601.1cm⁻¹ can be assigned to matrix site effect as this feature increased on annealing. The feature at 2577 cm⁻¹ can be assigned to Phac-D – H₂O adduct. When Phac-D was co-deposited with Methylamine and the matrix then annealed, a strong feature was obtained at 2516.6 cm⁻¹(Fig 3.1c and d, Grid A), which is red shifted by ~83 cm⁻¹ from the C-D stretching monomer feature. The feature at 1959.4, 1938.5 and 1928 cm⁻¹(Fig 3.1c and d, Grid B) arises only on complex formation and it is not shifted from any monomer feature of Phac-D in the spectra, computational calculations shows that this feature can be due to C≡C stretching mode .

In Fig 4.2a, the matrix isolation infrared spectra of Phac-D trapped in N₂ is shown. The spectral features at 757.5 cm⁻¹ is essentially due to C-D bending mode, which is also indicated by the computational calculation. When Phac-D was co-deposited with Methylamine and the matrix then annealed, a feature was obtained at 765.7 cm⁻¹(Fig 4.4d), which is blue shifted by ~8cm⁻¹ from the C-D bending monomer feature. The vibrational frequencies together with their assignment are presented in Table 4.6, 4.7 and 4.8 at B3LYP/6-311G++(d,p) and in Table 4.9, 4.10 and 4.11 at M062x/6-311G++(d,p), for C-D stretching, C≡C stretching and C-D bending modes, respectively.

While the computations predict that there are three different adducts that can possibly be formed between the two precursors, with three different frequencies for the Phac-D submolecule, we observe only one clear features in the C-D stretching region and three clear feature at C≡C stretching region. The question ofcourse is to identify which of the adducts are formed in the matrix. At the B3LYP/6-311G++(d,p) level, energy barrier of Complex 1 with Complex 2 and 3 is 1.24 kcal/mol and 2.07 kcal/mol, respectively, with Complex 1 being lower energy isomer. At M062x/6-311G++(d,p) level, the energy barrier between Complex 3 with Complex 1 and 3 is 0.0 and 0.2 kcal/mol, respectively, with Complex 2 and 3 being lower energy isomer. Therefore, from B3LYP/6-311G++(d,p) level of theory, energetics calculations rules out the possibility of Complex 2 and 3. From M062x/6-311G++(d,p) level of theory it is difficult to guess the experimental complex as the difference in energy calculations between the complexes is less.

From frequency calculations, at B3LYP/6-311G++(d,p) level, scaled frequencies of complex 1, 2 and 3 show red shift in the stretch of Phac-D submolecule of 85 cm⁻¹, 0.3 cm⁻¹ and 3 cm⁻¹, while experimentally we observe a red shift of 83cm⁻¹ (Table 4.6). At M062x/6-311G++(d,p) level, scaled frequencies of complex 1, 2 and 3 show red shift in the stretch of Phac-D submolecule of 85 cm⁻¹, 4 cm⁻¹ and 10 cm⁻¹, while experimentally we observe a red shift of 83 cm⁻¹ (Table 4.9). Therefore, there appears to be a better agreement of experimental and computed frequencies for Complex 1, which are the lowest energy conformers at B3LYP/6-311G++(d,p).

From frequency calculations, at B3LYP/6-311G++(d,p) level, scaled frequencies of complex 1, 2 and 3 show red shift in the C≡C stretch of Phac-D submolecule of 53 cm⁻¹, 0.6 cm⁻¹ and 7 cm⁻¹, while experimentally we do not observe C≡C stretching feature in the monomer and it can only be observed on complex formation. The calculations shows that

these features agrees well with Complex 1 and Complex 3 (Table 4.7). Similarly, at M062x/6-311G++(d,p) level, scaled frequencies of complex 1, 2, and 3 show red shift in the stretch of Phac-D submolecule of 53 cm^{-1} , 0.6 cm^{-1} , and 8 cm^{-1} and calculations shows that these features matches with Complex 1 and 3 (Table 4.10). Therefore, there appears to be a better agreement of experimental and computed frequencies for Complex 1 and Complex 3, which are the lowest energy conformers.

In the bend of Phac-D submolecule, frequency calculations, at B3LYP/6-311G++(d,p) level, scaled frequencies of complex 1, 2 and 3 show blue shift of 1.4 cm^{-1} , 2.2 cm^{-1} and 4.6 cm^{-1} , while experimentally we observe a blue shift of 6.5 cm^{-1} (Table 4.8). At M062x/6-311G++(d,p) level, scaled frequencies of complex 1 show blue shift of 33 cm^{-1} and Complex 2 and 3 show a red shift of 2.9 and 2.4 cm^{-1} , while experimentally we observe a blue shift of 6.5 cm^{-1} (Table 4.11). Therefore, from the experimental and computed frequencies it is difficult to assign the complex formed, but the appearance of this shift conforms the formation of the complex.

4.3.1.2 Features of Methylamine submolecule in the Phac-D – Methylamine adduct (s)

Fig 4.2b shows the matrix isolation infrared spectra of Methylamine trapped in N_2 . The spectral feature at 815.8 cm^{-1} is essentially due to N-H bending modes, which is also indicated by the computational calculations. When Phac-D was co-deposited with Methylamine and the matrix then annealed, a feature was obtained at 843 cm^{-1} (Fig 4.2d), which is blue shifted by $\sim 23\text{ cm}^{-1}$ from the N-H bending monomer feature. The vibrational frequencies together with their assignment are presented in Table 4.12 at B3LYP/6-311G++(d,p) and in Table 4.13 at M062x/6-311G++(d,p).

From frequency calculations, at B3LYP/6-311G++(d,p) level, scaled frequencies of complex 1, 2 and 3 show blue shift in the bending of Methylamine submolecule of 50 cm^{-1} , 14 cm^{-1} and 30 cm^{-1} , while experimentally we observe blue shift of 27 cm^{-1} (Table 4.12). At M062x/6-311G++(d,p) level, scaled frequencies of complex 1, 2 and 3 show blue shift in the bending of Methylamine submolecule of 33 cm^{-1} , 18 cm^{-1} and 26 cm^{-1} , while experimentally we observe a red shift of 27 cm^{-1} (Table 4.13). Therefore, from the experimental and computed frequencies, at B3LYP level, this feature is due to Complex 3; at M062x/6-311G++(d,p) it is difficult to assign the complex formed, but the appearance of this shift conforms the formation of the complex.

4.3.2 Experiments in Argon

4.3.2.1 Features of Phac-D sub molecule in the Phac-D – Methylamine adduct(s)

Fig 4.3a shows the matrix isolation infrared spectra of Phac-D trapped in Ar. The spectral features at 2607.7 cm^{-1} is essentially due to C-D stretching mode, which is also indicated by the computational calculation. The feature at 2597.8 cm^{-1} can be assigned to matrix site effect as this feature increased on annealing. The feature at 2574 cm^{-1} can be assigned to Phac-D – H_2O adduct. When Phac-D was co-deposited with Methylamine and the matrix then annealed, a strong feature was obtained at 2523.8 cm^{-1} (Fig 4.3c and d, Grid A), which is red shifted by $\sim 84\text{ cm}^{-1}$ from the C-D stretching monomer feature. The feature at 1960 and 1940 cm^{-1} (Fig 4.3c and d, Grid B) cannot be assigned from any spectral feature of Phac-D or Methylamine, from computation calculation this feature can be due to $\text{C}\equiv\text{C}$ stretching mode.

In Fig 4.4a, the matrix isolation infrared spectra of Phac-D trapped in Ar is shown. The spectral features at 757 cm^{-1} is essentially due to C-D bending mode, which is also indicated by the computational calculation. When Phac-D was co-deposited with Methylamine and the matrix then annealed, a feature was obtained at 765.7 cm^{-1} (Fig 4.4d), which is blue shifted by $\sim 9\text{ cm}^{-1}$ from the C-D bending monomer feature. The vibrational frequencies together with their assignment are presented in Table 4.14, 4.15 and 4.16 at B3LYP/6-311G++(d,p) and in Table 4.17, 4.18 and 4.19 at M062x/6-311G++(d,p) for C-D stretching, $\text{C}\equiv\text{C}$ stretching, and C-D bending modes, respectively.

From frequency calculations, at B3LYP/6-311G++(d,p) level, scaled frequencies of complex 1, 2 and 3 show red shift in the stretch of Phac-D submolecule of 85 cm^{-1} , 0.4 cm^{-1} and 3 cm^{-1} , while experimentally we observe a red shift of 84 cm^{-1} (Table 4.14). At M062x/6-311G++(d,p) level, scaled frequencies of complex 1, 2 and 3 show red shift in the stretch of Phac-D submolecule of 85 cm^{-1} , 4 cm^{-1} and 10 cm^{-1} , while experimentally we observe a red shift of 84 cm^{-1} (Table 4.17). Therefore, there appears to be a better agreement of experimental and computed frequencies for Complex 1, which are the lowest energy conformers at B3LYP/6-311G++(d,p).

From frequency calculations, at B3LYP/6-311G++(d,p) level, scaled frequencies of complex 1, 2 and 3 show red shift in the $\text{C}\equiv\text{C}$ stretch of Phac-D submolecule of 50 cm^{-1} , 0.7 cm^{-1} and 5 cm^{-1} , while experimentally we do not observe $\text{C}\equiv\text{C}$ stretching feature in the monomer and it can only be observed on complex formation. The calculations shows that

these features agrees well with Complex 1 and Complex 3 (Table 4.15). Similarly, at M062x/6-311G++(d,p) level, scaled frequencies of complex 1, 2, and 3 show red shift in the stretch of Phac-D submolecule of 55 cm^{-1} , 0.6 cm^{-1} , and 8 cm^{-1} and calculations shows that these features matches with Complex 1 and 3 (Table 4.18). Therefore, there appears to be a better agreement of experimental and computed frequencies for Complex 1 and Complex 3, which are the lowest energy complexes.

In the bend of Phac-D submolecule, frequency calculations, at B3LYP/6-311G++(d,p) level, scaled frequencies of complex 1, 2 and 3 show blue shift of 0.6 cm^{-1} , 1.7 cm^{-1} and 4.6 cm^{-1} , while experimentally we observe a blue shift of 8 cm^{-1} (Table 4.16). At M062x/6-311G++(d,p) level, scaled frequencies of complex 1 show blue shift of 33 cm^{-1} and Complex 2 and 3 show a red shift of 2.9 and 2.4 cm^{-1} , while experimentally we observe a blue shift of 8 cm^{-1} (Table 4.19). Therefore, from the experimental and computed frequencies it is difficult to assign the complex formed, but the appearance of this shift conforms the formation of the complex.

4.3.2.2 Features of Methylamine submolecule in the Phac-D – Methylamine adduct (s)

Fig 4.4b shows the matrix isolation infrared spectra of Methylamine trapped in Ar. The spectral feature at 796.5 cm^{-1} is essentially due to N-H bending mode, which is also indicated by the computational calculation. When Phac-D was co-deposited with Methylamine and the matrix then annealed, a feature was obtained at 810.5 cm^{-1} (Fig 4.4d), which is blue shifted by $\sim 15\text{ cm}^{-1}$ from the N-H bending monomer feature. The vibrational frequencies together with their assignment are presented in Table 4.20 at B3LYP/6-311G++(d,p) and in Table 4.21 at M062x/6-311G++(d,p).

From frequency calculations, at B3LYP/6-311G++(d,p) level, scaled frequencies of complex 1, 2 and 3 show blue shift in the bending of Methylamine submolecule of 48 cm^{-1} , 14 cm^{-1} and 29 cm^{-1} , while experimentally we observe blue shift of 14 cm^{-1} (Table 4.20). At M062x/6-311G++(d,p) level, scaled frequencies of complex 1, 2 and 3 show blue shift in the bending of Methylamine submolecule of 33 cm^{-1} , 18 cm^{-1} and 31 cm^{-1} , while experimentally we observe a blue shift of 14 cm^{-1} (Table 4.21). Therefore, from the experimental and computed frequencies this feature agrees well with Complex 2.

4.4 AIM Analysis

An examination of the charge density topology was performed using the atoms-in-molecules (AIM) theory of Bader. (3, -1) bond critical points (BCP) that could be associated with complexes 1, 2 and 3 were located as shown in Fig 4.7 at B3LYP/6-311G++(d,p) and in Fig 4.8 at M062x/6-311G++(d,p). The electron density ($\rho(r_c)$) and Laplacian of electron density $\nabla^2\rho(r_c)$ were computed for the critical points and the values are shown in Table 4.22 at B3LYP/6-311G++(d,p) and in Table 4.23 at M062x/6-311G++(d,p). The $\rho(r_c)$ and $\nabla^2\rho(r_c)$ values for bond critical points in both the complexes were found to be in the order of 10^{-2} au.

At B3LYP/6-311G++(d,p) level, in complex 3 a secondary interaction was also present between N of methylamine and H of benzene ring in Phac-D. At M062x/6-311G++(d,p) level, in Complex 2 a secondary interaction was between methyl group of Methylamine and C of benzene ring in Phac-D, and in Complex 3 a secondary interaction was between N of methylamine and H of benzene ring in Phac-D and a tertiary interaction between methyl group of methylamine and acetylenic π of benzene. The secondary and tertiary interactions are mentioned as BCP2 and BCP3 in Table 4.22 at B3LYP/6-311G++(d,p) and in Table 4.23 at M062x/6-311G++(d,p).

4.5 Conclusion

The infrared spectra of Phac-D and Methylamine trapped in solid N_2 and Ar, were studied. The experiments and computations clearly indicate the formation of Complex 1. The B3LYP/6-311G++(d,p) level of theory indicates that the energy barrier between Complex 1 with Complex 2 and 3 is more than 1kcal/mol, therefore Complex 1 have formed in the experiment. Frequency shifts calculation does not show any significant shift for Complex 2 but energy calculations does not rule out the possibility of its existence. At M062x/6-311G++(d,p) level of theory the energy barrier between Complex 2 with Complex 1 and 3 is less and therefore, the other complexes might exist in the experiment but from frequency shift they are difficult to assign.

**TABLE 4.1: Stabilization Energy for Phac-D and Methylamine Complexes
(Raw/ZP/BSSE) in kcal mol⁻¹**

Structures of Phac-D and Methylamine	B3LYP/6-311G++(d,p)	M062x/6-311G++(d,p)
Complex1	-3.56/-2.42/-3.08	-4.7/-3.7/-4.2
Complex2	-0.75/-0.35/-0.53	-4.5/-3.5/-3.9
Complex3	-1.93/-1.18/-1.67	-4.7/-3.7/-4.3

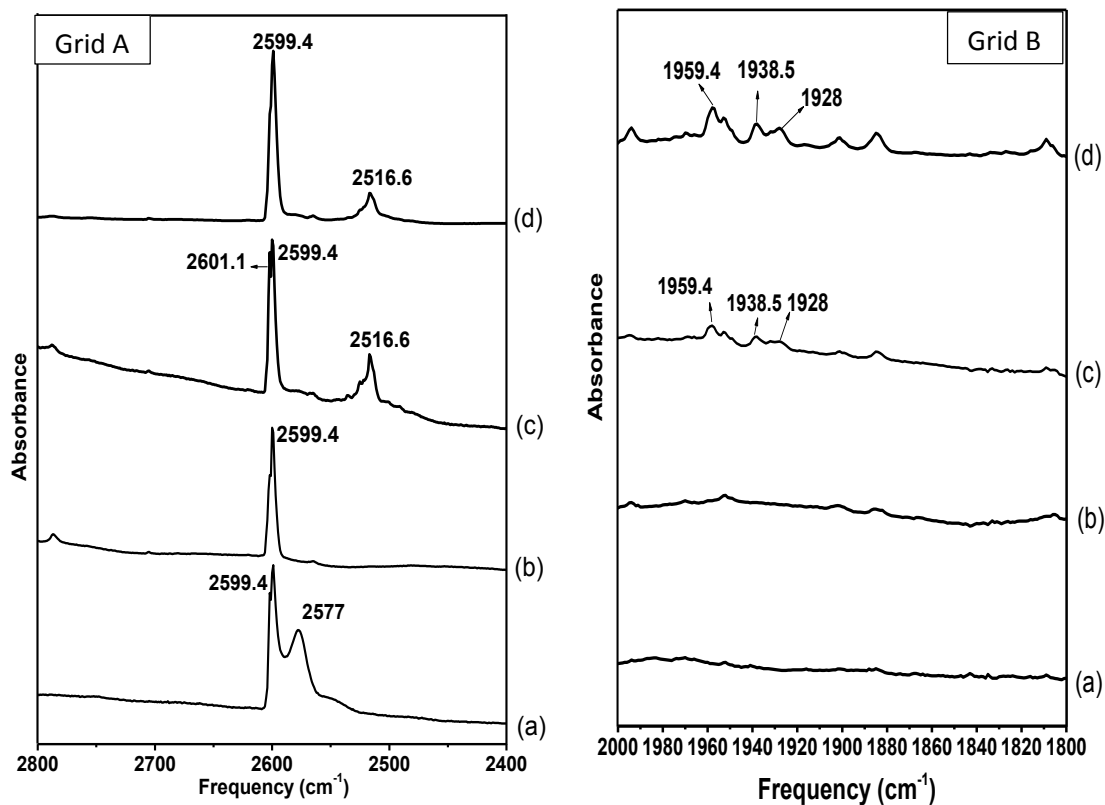


Fig 4.1: IR Spectra of Phac-D and Methylamine in Nitrogen, the spectra spans the region from 2800-2400cm⁻¹ and 900-700cm⁻¹, (a) Phac-D alone (1:1000) annealed at 32K, (b) Phac-D : Methylamine at 12K (1:1), (c) Phac-D: Methylamine annealed at 32K and then brought back to 12K (1:1), (d) Phac-D: Methylamine annealed at 32K and then brought back to 12K (3:1).

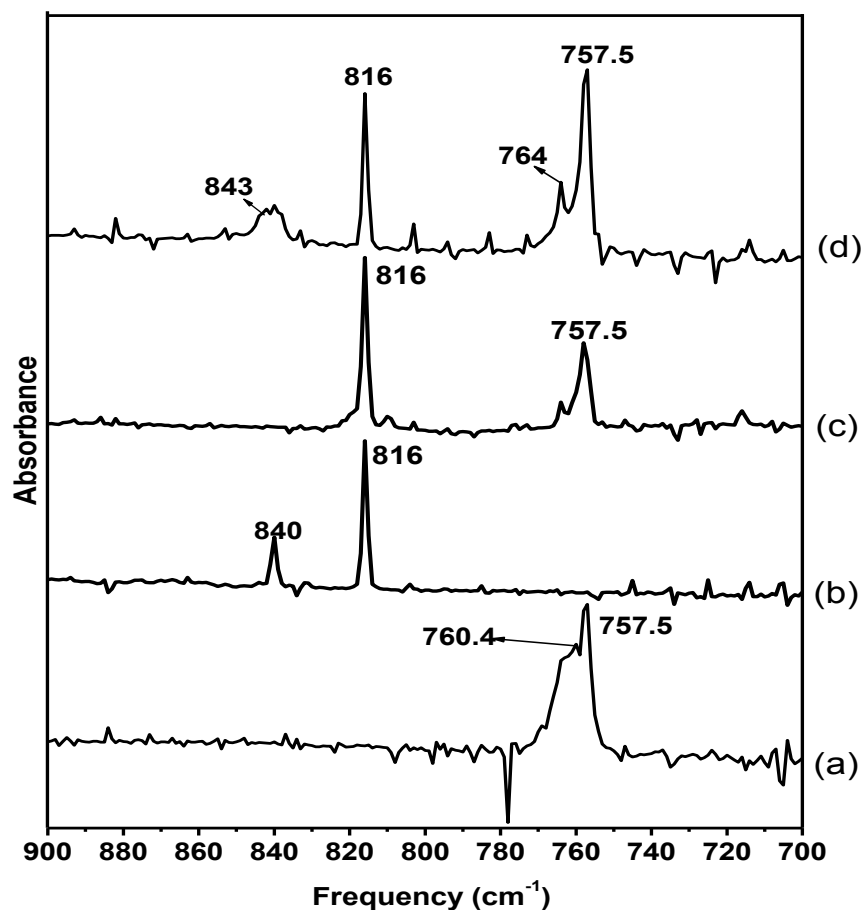


Fig 4.2: IR Spectra of Phac-D and Methanol in Nitrogen, the spectra spans the region from 4000-3500cm⁻¹, (a) Phac-D alone (1:1000) annealed at 32K, (b) Methylamine alone (1:1000) annealed at 32K, (c) Phac-D: Methylamine(1:1) at 12K, (d) Phac-D: Methylamine annealed at 32K and then brought back to 12K (1:1).

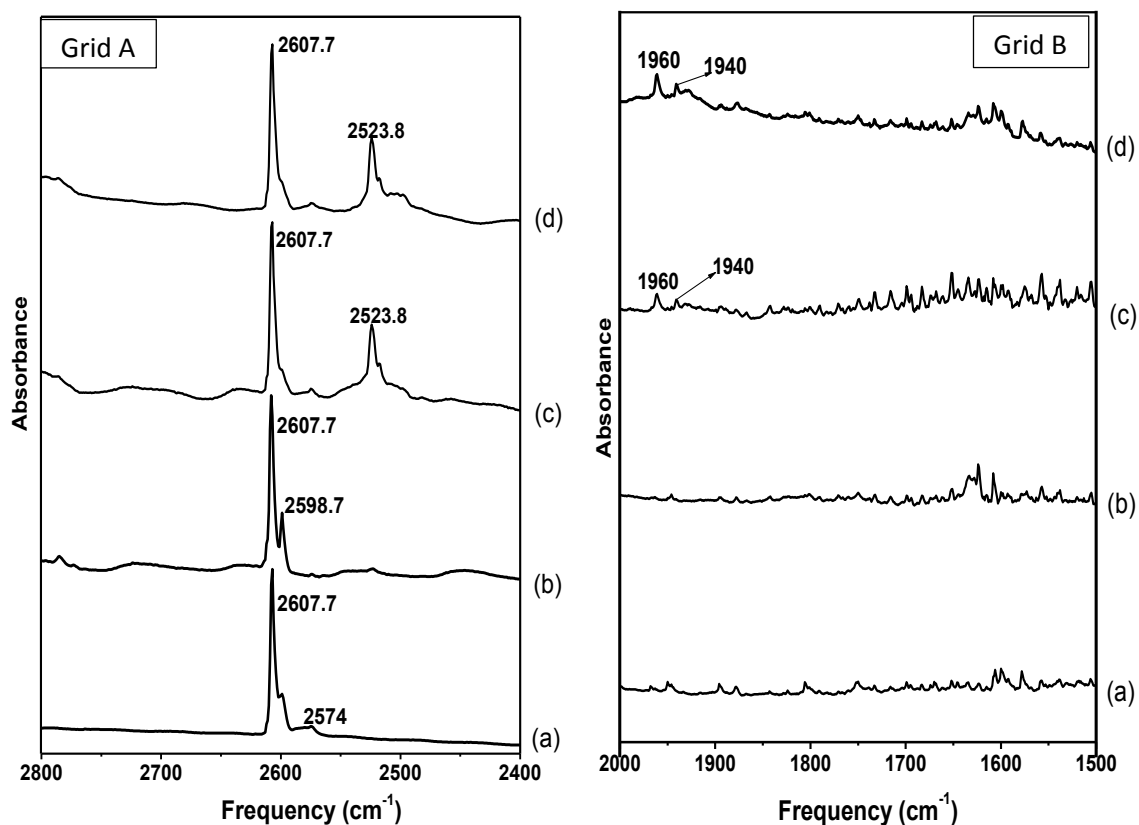


Fig 4.3: IR Spectra of Phac-D and Methylamine in Nitrogen, the spectra spans the region from 2800-2400cm⁻¹ and 900-700cm⁻¹, (a) Phac-D alone (3:1000) annealed at 35K, (b) Phac-D : Methylamine at 12K (3:1.2), (c) Phac-D: Methylamine annealed at 35K and then brought back to 12K (3:1.2), (d) Phac-D: Methylamine annealed at 35K and then brought back to 12K (3:1.4).

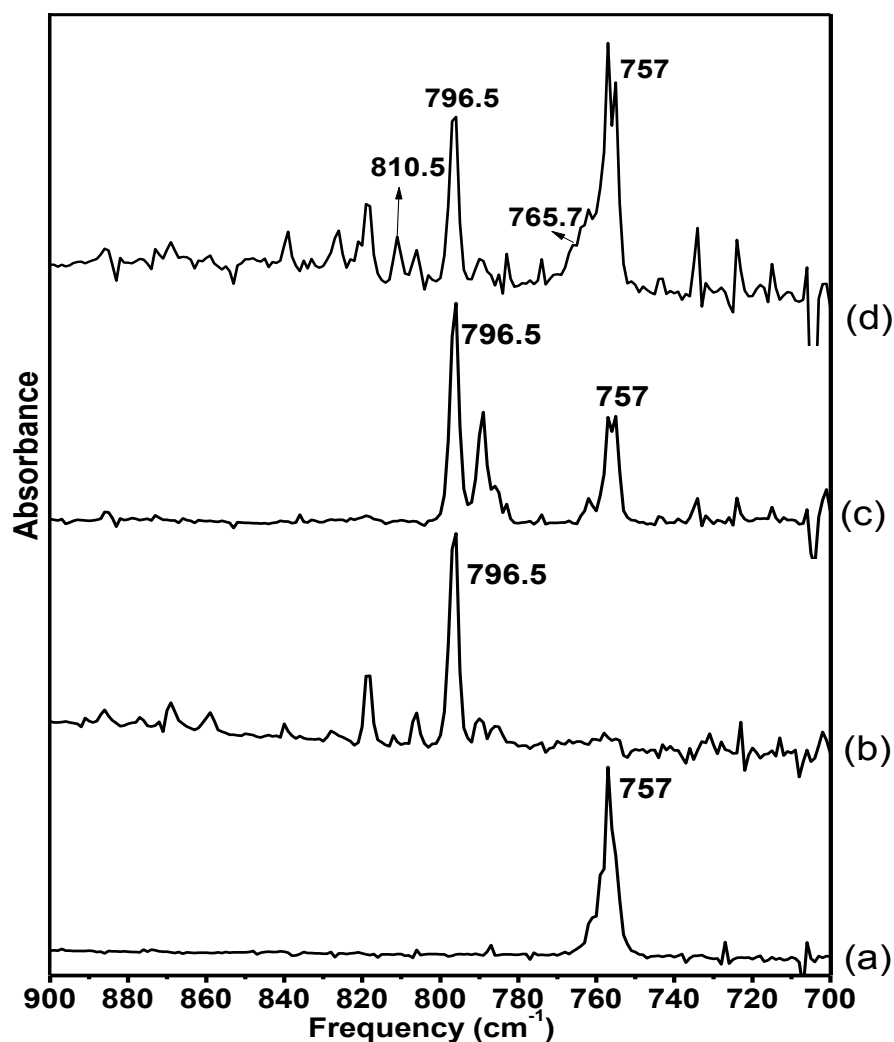
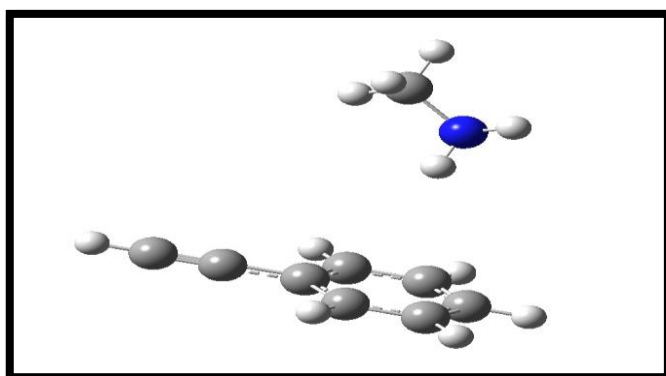


Fig 4.4: IR Spectra of Phac-D and Methanol in Nitrogen, the spectra spans the region from 4000-3500cm⁻¹, (a) Phac-D alone (3:1000) annealed at 35K, (b) Methylamine alone (1.2:1000) annealed at 35K, (c) Phac-D: Methylamine (3:1.2) at 12K, (d) Phac-D: Methylamine annealed at 35K and then brought back to 12K (3:1.2).

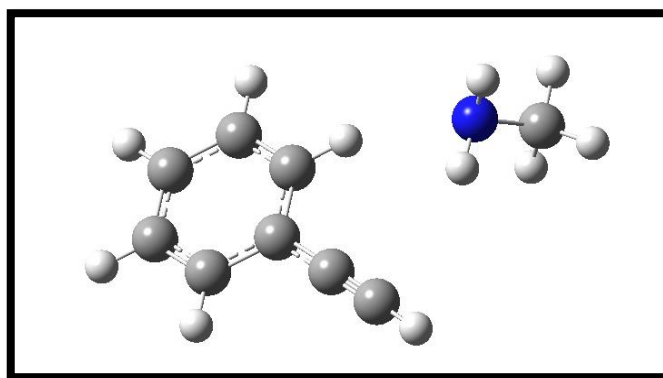


Raw	ZP	BSSE
-0.75	-0.35	-0.53

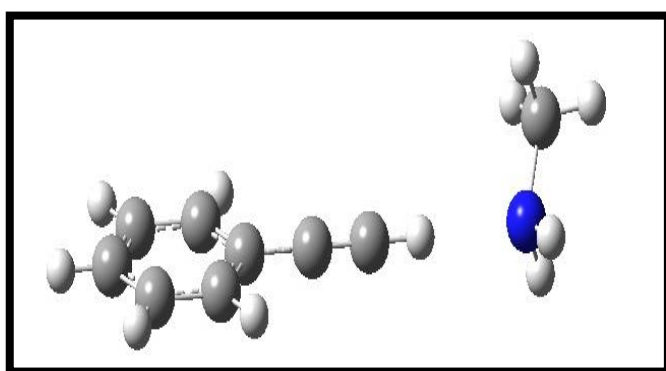
Complex2

*Stabilization Energy
In kcal mol⁻¹*

Raw	ZP	BSSE
-1.93	-1.18	-1.67



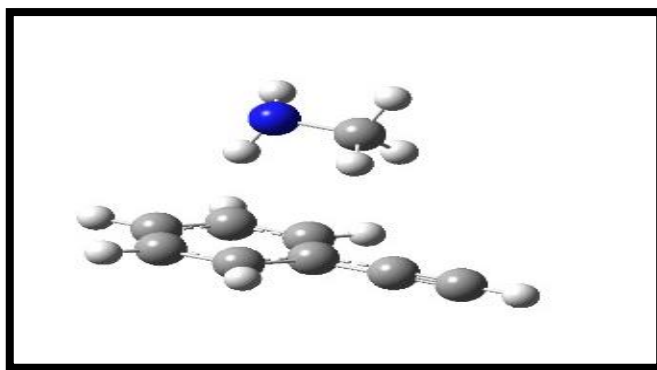
Complex3



Raw	ZP	BSSE
-3.56	-2.42	-3.08

Complex1

Fig 4.5: Complex structure between Phac-D and Methylamine at B3LYP/6-31G++(d,p) with stabilization energy

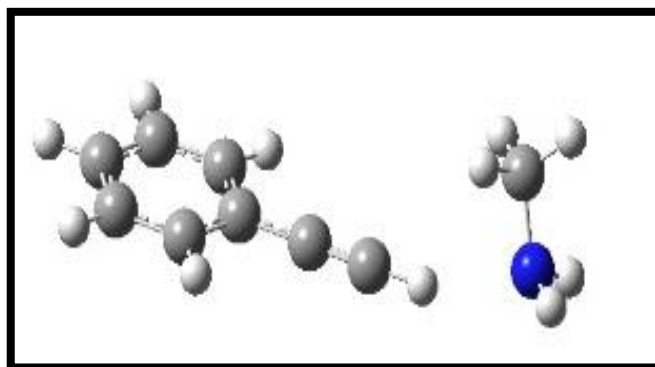


Raw	ZP	BSSE
-4.5	-3.5	-3.9

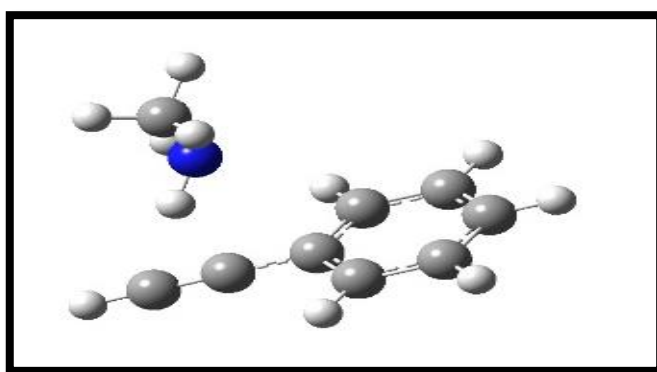
Complex2

*Stabilization Energy
In kcal mol⁻¹*

Raw	ZP	BSSE
-4.7	-3.7	-4.2



Complex1



Raw	ZP	BSSE
-4.7	-3.7	-4.3

Complex3

Fig 4.6: Complex structure between Phac-D and Methylamine at B3LYP/6-311G++(d,p) with stabilization energy

Table 4.2: Some selected geometrical parameters of Complex 1 at B3LYP/6-311G++(d,p) and M062x/6-311G++(d,p) where bond length is given in Å , bond angle in degree(°) and torsional angles in degree(°)

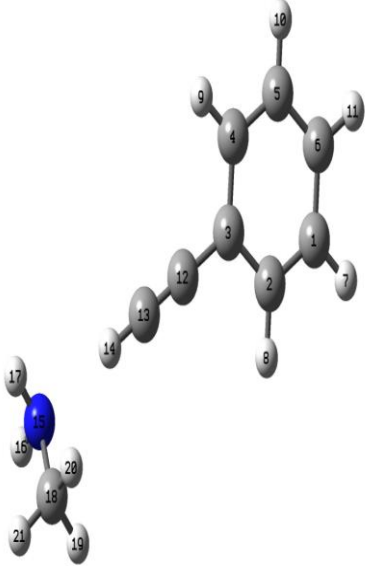
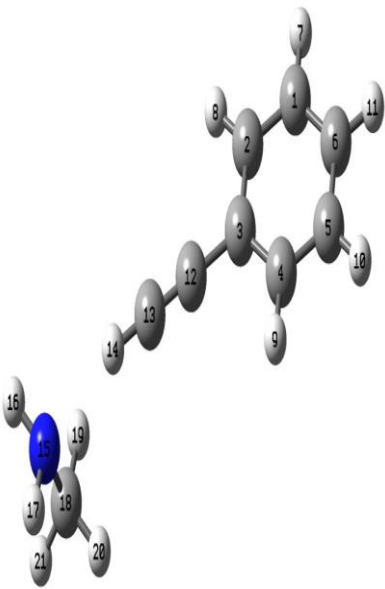
Complex 1	B3LYP/6-311G++(d,p)	M062x/6-311G++(d,p)
		
D14-N15	2.3	2.2
D14-C13	1.1	1.1
C13-D14-N15	177.9	158.5
H17-N15-D14	109.5	119.1
H16-N15-D14	160.9	116.3
C18-N15-D14	110	92.4
H17-N15-D14-C13	117	121.5
H16-N15-D14-C13	-127	-108.5
C18-N15-D14-C13	-5	6

Table 4.3: Some selected geometrical parameters of Complex 2 at B3LYP/6-311G++(d,p) and M062x/6-311G++(d,p) where bond length is given in Å , bond angle in degree(°) and torsional angles in degree(°)

Complex 2	B3LYP/6-311G++(d,p)	M062x/6-311G++(d,p)
C1-H21	3.0	2.7
C2-H21	3.0	2.8
C3-H17	5.0	3.1
C3-H18	5.2	3.0
N19-H21-C1	144.4	166
N19-H21-C2	154	140
H21-C1-C2	78.4	77.3
H21-C2-C1	74.8	73
N19-H21-C1-C2	-131	-49.4
N19-H21-C2-C1	93.2	163.1

Table 4.4: Some selected geometrical parameters of Complex 3 at B3LYP/6-311G++(d,p) and M062x/6-311G++(d,p) where bond length is given in Å , bond angle in degree(°) and torsional angles in degree(°)

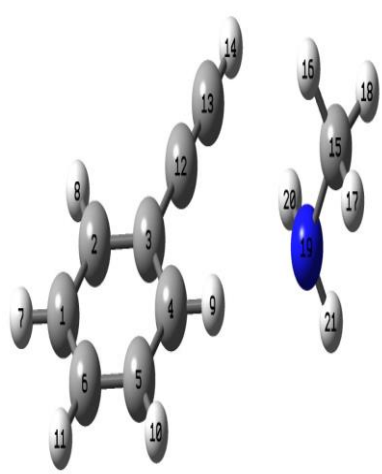
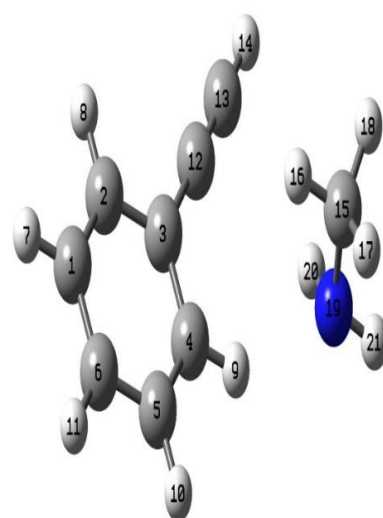
Complex 3	B3LYP/6-311G++(d,p)	M062x/6-311G++(d,p)
		
C12-H20	3.0	2.8
C13-H20	2.9	2.7
N19-H9	2.5	2.4
H16-C12	4.5	2.9
H16-C13	4.6	3.2
N19-H20-C12	135	120
N19-H20-C13	159	138
N19-H9-C4	160	147.6
N19-H20-C12-C13	179	143
N19-H20-C13-C12	-2.0	-52
H20-N19-H9-C4	-1.45	-60

Table 4.5: Calculated and experimental frequency table for shifts (cm⁻¹) in Phenylacetylene-D (Phac-D) C-D stretching due to the formation of Phenylacetylene-D and Methylamine complexes in N₂ matrix at B3LYP/6-311G++(d,p)

<u>Nitrogen</u>	<u>Unscaled Freq.</u>	<u>Scaled Freq.</u>	<u>Scaling Factor</u>	<u>Exptl. Freq.</u>	<u>Δv (exp-scaled)</u>	<u>Mode of assignment</u>
<u>Phac-D</u>	2711.7	2599.4		2599.4		C-D stretching
<u>Complex1</u>	2623.4	2514.8	0.9586	2516.6	1.8	C-D stretching
<u>Complex2</u>	2711.4	2599.1	0.9586			C-D stretching
<u>Complex3</u>	2708.2	2596.1	0.9586			C-D stretching

Table 4.6: Calculated and experimental frequency table for shifts (cm⁻¹) in Phenylacetylene-D (Phac-D) C≡C stretching due to the formation of Phenylacetylene-D and Methylamine complexes in N₂ matrix at B3LYP/6-311G++(d,p)

<u>Nitrogen</u>	<u>Unscaled Freq.</u>	<u>Scaled Freq.</u>	<u>Scaling Factor</u>	<u>Exptl. Freq.</u>	<u>Δv (exp-scaled)</u>	<u>Mode of assignment</u>
<u>Phac-D</u>	2058.9	1973.6				C≡C stretching
<u>Complex 1</u>	2005.5	1922.5	0.9586	1928, 1938.5	5.5, 16	C≡C stretching
<u>Complex 2</u>	2059.0	1973.8	0.9586			C≡C stretching
<u>Complex 3</u>	2053.5	1968.5	0.9586	1959.4	8.9	C≡C stretching

Table 4.7: Calculated and experimental frequency table for shifts (cm⁻¹) in Phenylacetylene-D (Phac-D) C-D bending due to the formation of Phenylacetylene-D and Methylamine complexes in N₂ matrix at B3LYP/6-311G++(d,p)

<u>Nitrogen</u>	<u>Unscaled Freq.</u>	<u>Scaled Freq.</u>	<u>Scaling Factor</u>	<u>Exptl. Freq.</u>	<u>Δv (exp-scaled)</u>	<u>Mode of assignment</u>
<u>Phac-D</u>	773.3	757.5		757.5		C-D bending
<u>Complex 1</u>	773.9	758.1	0.9796	764	5.9	C-D bending
<u>Complex 2</u>	775.1	759.3	0.9796	764	4.7	C-D bending
<u>Complex 3</u>	778	762.1	0.9796	764	1.9	C-D bending

Table 4.8: Calculated and experimental frequency table for shifts (cm⁻¹) in Phenylacetylene-D (Phac-D) C-D stretching due to the formation of Phenylacetylene-D and Methylamine complexes in N₂ matrix at M062x/6-311G++(d,p)

<u>Nitrogen</u>	<u>Unscaled Freq.</u>	<u>Scaled Freq.</u>	<u>Scaling Factor</u>	<u>Exptl. Freq.</u>	<u>Δv (exp-scaled)</u>	<u>Mode of assignment</u>
<u>Phac-D</u>	2740	2599.4		2599.4		C-D stretching
<u>Complex1</u>	2650.1	2514.1	0.9487	2516.6	2.5	C-D stretching
<u>Complex2</u>	2735.3	2595.0	0.9487			C-D stretching
<u>Complex3</u>	2729	2589.0	0.9487			C-D stretching

Table 4.9: Calculated and experimental frequency table for shifts (cm⁻¹) in Phenylacetylene-D (Phac-D) C \equiv C stretching due to the formation of Phenylacetylene-D and Methylamine complexes in N₂ matrix at M062x/6-311G++(d,p)

<u>Nitrogen</u>	<u>Unscaled Freq.</u>	<u>Scaled Freq.</u>	<u>Scaling Factor</u>	<u>Exptl. Freq.</u>	<u>Δv (exp-scaled)</u>	<u>Mode of assignment</u>
<u>Phac-D</u>	2090.7	1983.4				C \equiv C stretching
<u>Complex1</u>	2033.4	1929.1	0.9487	1928, 1938.5	-1.1, 9.4	C \equiv C stretching
<u>Complex2</u>	2090.0	1982.8	0.9487			C \equiv C stretching
<u>Complex3</u>	2082.6	1975.8	0.9487	1959.4	-16.4	C \equiv C stretching

Table 4.10: Calculated and experimental frequency table for shifts (cm⁻¹) in Phenylacetylene-D (Phac-D) C-D bending due to the formation of Phenylacetylene-D and Methylamine complexes in N₂ matrix at M062x/6-311G++(d,p)

<u>Nitrogen</u>	<u>Unscaled Freq.</u>	<u>Scaled Freq.</u>	<u>Scaling Factor</u>	<u>Exptl. Freq.</u>	<u>$\Delta\nu$ (exp-scaled)</u>	<u>Mode of assignment</u>
<u>Phac-D</u>	784.3	757.5		757.5		C-D bending
<u>Complex 1</u>	818.8	790.8	0.9658	764	13.2	C-D bending
<u>Complex 2</u>	781.3	754.6	0.9658	764	9.4	C-D bending
<u>Complex 3</u>	781.8	755.1	0.9658	764	8.9	C-D bending

Table 4.11: Calculated and experimental frequency table for shifts (cm⁻¹) in Methylamine N-H bending frequency due to the formation of Phenylacetylene-D and Methylamine complexes in N₂ matrix at B3LYP/6-311G++(d,p)

<u>Nitrogen</u>	<u>Unscaled Freq.</u>	<u>Scaled Freq.</u>	<u>Scaling Factor</u>	<u>Exptl. Freq.</u>	<u>Δv (exp-scaled)</u>	<u>Mode of assignment</u>
<u>NH₂CH₃</u>	823.4	816		816		N-H bending
<u>Complex 1</u>	873.4	865.5	0.991			N-H bending
<u>Complex 2</u>	837.7	830.2	0.991			N-H bending
<u>Complex 3</u>	853.3	845.6	0.991	843	-2.6	N-H bending

Table 4.12: Calculated and experimental frequency table for shifts (cm⁻¹) in Methylamine N-H bending frequency due to the formation of Phenylacetylene-D and Methylamine complexes in N₂ matrix at M062x/6-311G++(d,p)

<u>Nitrogen</u>	<u>Unscaled Freq.</u>	<u>Scaled Freq.</u>	<u>Scaling Factor</u>	<u>Exptl. Freq.</u>	<u>Δv (exp-scaled)</u>	<u>Mode of assignment</u>
<u>NH₂CH₃</u>	835.3	816		816		N-H bending
<u>Complex 1</u>	868.9	848.8	0.9769	843	-5.8	N-H bending
<u>Complex 2</u>	854.1	834.4	0.9769	843	8.6	N-H bending
<u>Complex 3</u>	867.6	847.6	0.9769	843	-4.6	N-H bending

Table 4.13: Calculated and experimental frequency table for shifts (cm⁻¹) in Phenylacetylene-D (Phac-D) C-D stretching due to the formation of Phenylacetylene-D and Methylamine complexes in Ar matrix at B3LYP/6-311G++(d,p)

<u>Argon</u>	<u>Unscaled Freq.</u>	<u>Scaled Freq.</u>	<u>Scaling Factor</u>	<u>Exptl. Freq.</u>	<u>Δv (exp-scaled)</u>	<u>Mode of assignment</u>
<u>Phac-D</u>	2711.7	2607.7		2607.7		C-D stretching
<u>Complex1</u>	2623.4	2522.7	0.9616	2523.8	1.1	C-D stretching
<u>Complex2</u>	2711.4	2607.3	0.9616			C-D stretching
<u>Complex3</u>	2708.2	2604.2	0.9616			C-D stretching

Table 4.14: Calculated and experimental frequency table for shifts (cm⁻¹) in Phenylacetylene-D (Phac-D) C≡C stretching due to the formation of Phenylacetylene-D and Methylamine complexes in Ar matrix at B3LYP/6-311G++(d,p)

<u>Argon</u>	<u>Unscaled Freq.</u>	<u>Scaled Freq.</u>	<u>Scaling Factor</u>	<u>Exptl. Freq.</u>	<u>Δv (exp-scaled)</u>	<u>Mode of assignment</u>
<u>Phac-D</u>	2058.9	1979.3				C≡C stretching
<u>Complex1</u>	2005.5	1928.5	0.9616	1940	11.5	C≡C stretching
<u>Complex2</u>	2059.0	1980	0.9616			C≡C stretching
<u>Complex3</u>	2053.5	1974.6	0.9616	1960	-14.6	C≡C stretching

Table 4.15: Calculated and experimental frequency table for shifts (cm⁻¹) in Phenylacetylene-D (Phac-D) C-D bending due to the formation of Phenylacetylene-D and Methylamine complexes in Ar matrix at B3LYP/6-311G++(d,p)

<u>Argon</u>	<u>Unscaled Freq.</u>	<u>Scaled Freq.</u>	<u>Scaling Factor</u>	<u>Exptl. Freq.</u>	<u>$\Delta\nu$ (exp-scaled)</u>	<u>Mode of assignment</u>
<u>Phac-D</u>	773.3	757		757		C-D bending
<u>Complex1</u>	773.9	757.6	0.9789	765.7	8.1	C-D bending
<u>Complex2</u>	775.1	758.7	0.9789	765.7	7	C-D bending
<u>Complex3</u>	778	761.6	0.9789	765.7	4.1	C-D bending

Table 4.16: Calculated and experimental frequency table for shifts (cm⁻¹) in Phenylacetylene-D (Phac-D) C-D stretching due to the formation of Phenylacetylene-D and Methylamine complexes in Ar matrix at M062x/6-311G++(d,p)

<u>Argon</u>	<u>Unscaled Freq.</u>	<u>Scaled Freq.</u>	<u>Scaling Factor</u>	<u>Exptl. Freq.</u>	<u>Δv (exp-scaled)</u>	<u>Mode of assignment</u>
<u>Phac-D</u>	2740	2607.7		2607.7		C-D stretching
<u>Complex1</u>	2650.1	2522.1	0.9517	2523.8	1.7	C-D stretching
<u>Complex2</u>	2735.3	2603.2	0.9517			C-D stretching
<u>Complex3</u>	2729	2597.2	0.9517			C-D stretching

Table 4.17: Calculated and experimental frequency table for shifts (cm⁻¹) in Phenylacetylene-D (Phac-D) C≡C stretching due to the formation of Phenylacetylene-D and Methylamine complexes in Ar matrix at M062x/6-311G++(d,p)

<u>Argon</u>	<u>Unscaled Freq.</u>	<u>Scaled Freq.</u>	<u>Scaling Factor</u>	<u>Exptl. Freq.</u>	<u>Δv (exp-scaled)</u>	<u>Mode of assignment</u>
<u>Phac-D</u>	2090.7	1989.7				C≡C stretching
<u>Complex 1</u>	2033.4	1935.2	0.9517	1940	4.8	C≡C stretching
<u>Complex 2</u>	2090.0	1989.1	0.9517			C≡C stretching
<u>Complex 3</u>	2082.6	1982.0	0.9517	1960	22	C≡C stretching

Table 4.18: Calculated and experimental frequency table for shifts (cm⁻¹) in Phenylacetylene-D (Phac-D) C-D bending due to the formation of Phenylacetylene-D and Methylamine complexes in Argon matrix at M062x/6-311G++(d,p)

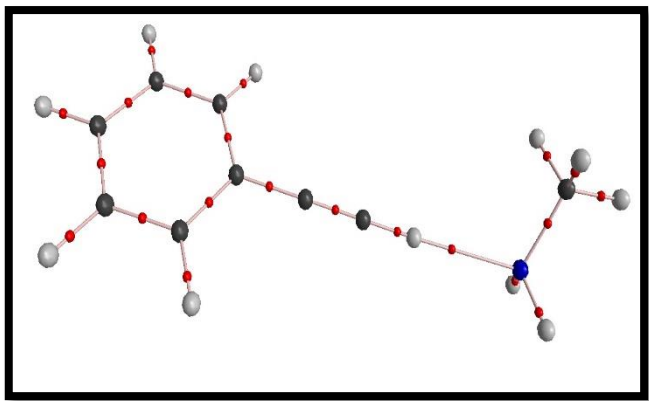
<u>Argon</u>	<u>Unscaled Freq.</u>	<u>Scaled Freq.</u>	<u>Scaling Factor</u>	<u>Exptl. Freq.</u>	<u>$\Delta\nu$ (exp-scaled)</u>	<u>Mode of assignment</u>
<u>Phac-D</u>	784.3	757		757		C-D bending
<u>Complex 1</u>	818.8	790.3	0.9652	765.7	-15.4	C-D bending
<u>Complex 2</u>	781.3	754.1	0.9652	765.7	11.6	C-D bending
<u>Complex 3</u>	781.8	754.6	0.9652	765.7	11.1	C-D bending

Table 4.19: Calculated and experimental frequency table for shifts (cm⁻¹) in Methylamine N-H bending frequency due to the formation of Phenylacetylene-D and Methylamine complexes in Argon matrix at B3LYP/6-311G++(d,p)

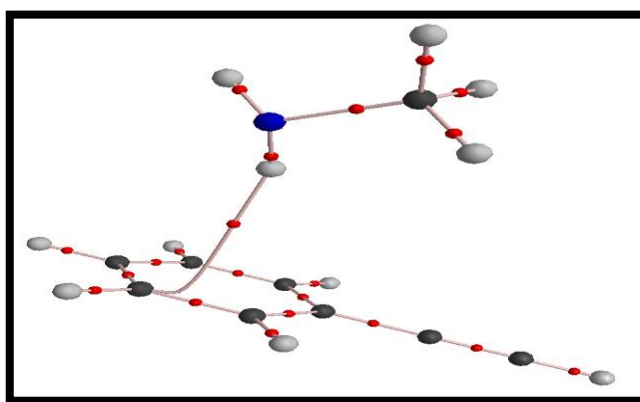
<u>Argon</u>	<u>Unscaled Freq.</u>	<u>Scaled Freq.</u>	<u>Scaling Factor</u>	<u>Exptl. Freq.</u>	<u>Δv (exp-scaled)</u>	<u>Mode of assignment</u>
<u>NH₂CH₃</u>	823.4	796.5		796.5		N-H bending
<u>Complex 1</u>	873.4	844.8	0.9673			N-H bending
<u>Complex 2</u>	837.7	810.3	0.9673	810.5	0.2	N-H bending
<u>Complex 3</u>	853.3	825.4	0.9673			N-H bending

Table 4.20: Calculated and experimental frequency table for shifts (cm⁻¹) in Methylamine N-H stretching frequency due to the formation of Phenylacetylene-D and Methylamine complexes in Ar matrix at M062x/6-311G++(d,p)

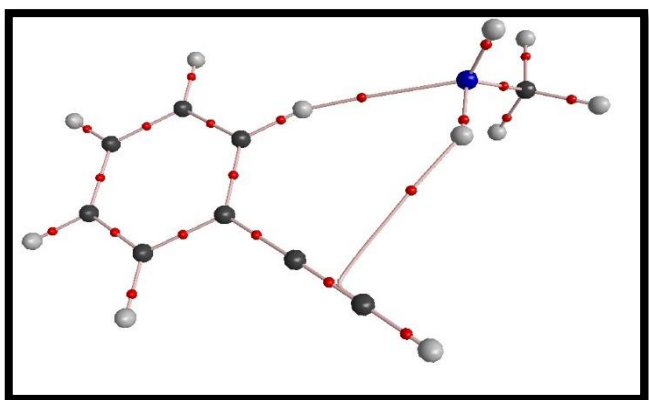
<u>Argon</u>	<u>Unscaled Freq.</u>	<u>Scaled Freq.</u>	<u>Scaling Factor</u>	<u>Exptl. Freq.</u>	<u>Δv (exp-scaled)</u>	<u>Mode of assignment</u>
<u>NH₂CH₃</u>	835.3	796.5		796.5		N-H bending
<u>Complex1</u>	868.9	828.5	0.9535			N-H bending
<u>Complex2</u>	854.1	814.4	0.9535	810.5	3.9	N-H bending
<u>Complex 3</u>	867.6	827.3	0.9535			N-H bending



Complex1

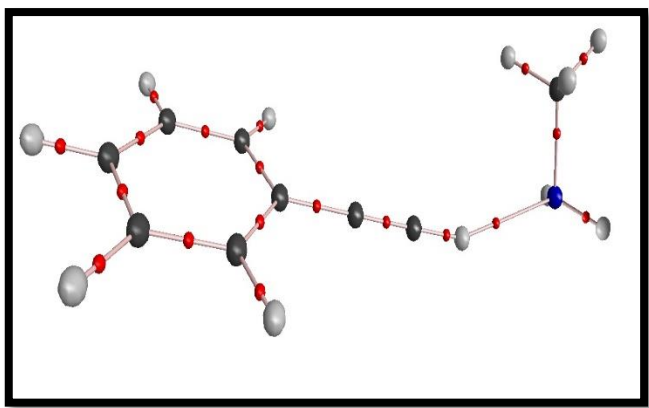


Complex2

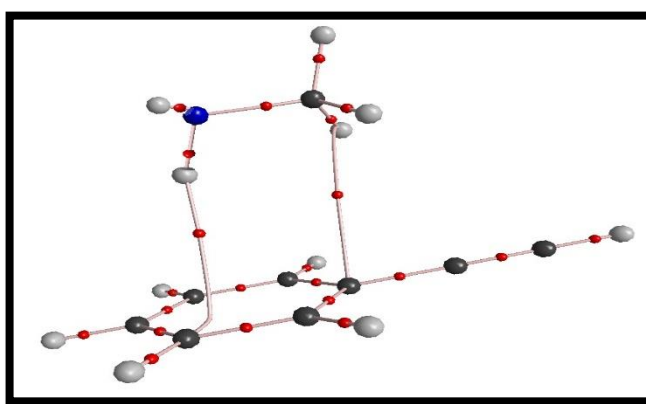


Complex3

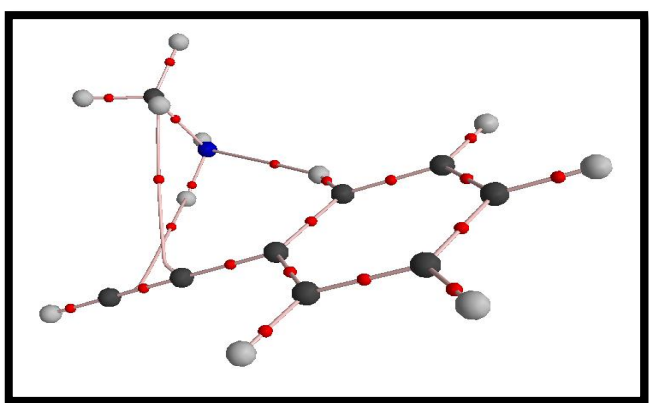
Fig 4.7: AIM analysis at B3LYP/6-311G++(d,p) level



Complex1



Complex2



Complex3

Fig 4.8: AIM analysis at B3LYP/6-311G++(d,p) level

Table 4.22 – Properties of different critical points present in Phac-D and Methylamine complexes as a result of AIM analysis in B3LYP/6-311G++(d,p)

Complex	Critical Point	$\rho(\mathbf{rc})$	$\nabla^2\rho(\mathbf{rc})$
Complex 1	BCP	0.01675	-0.01229
Complex 2	BCP	0.00428	-0.00283
Complex 3	BCP1	0.00527	-0.00345
	BCP2	0.01071	-0.00721

Table 4.23 – Properties of different critical points present in Phac-D and Methylamine complexes as a result of AIM analysis in M062x/6-311G++(d,p).

Complex	Critical Point	$\rho(\mathbf{rc})$	$\nabla^2\rho(\mathbf{rc})$
Complex 1	BCP	0.02235	-0.04125
Complex 2	BCP1	0.00718	-0.00568
	BCP2	0.00630	-0.00535
Complex 3	BCP1	0.00798	-0.00594
	BCP2	0.01330	-0.01047
	BCP3	0.00568	-0.00425

Chapter 5

SUMMARY AND CONCLUSIONS

This thesis discussed our results on our studies on the reaction of Phac-D with methanol and methylamine. This thesis presents the studies and interaction on the complexes of Phac-D with methanol and methylamine using matrix isolation infrared and ab-initio calculations both in low temperature and in the gas phase, where the switching from O-H to N-H group has been studied.

To understand the nature of the interaction between Phac-D and methanol, the submolecules were separately co-deposited in the N₂ and Ar matrix. This resulted in two hydrogen bonded complex, which was evidenced by the shifts in the vibrational frequencies of Phac-D and Methanol submolecules. While our computations indicated three minima at B3LYP/6-311G++(d,p)) and four minima at M062x/6-311G++(d,p) minima for the Phac-D and Methanol adducts, only two adducts were experimentally identified in the matrix at low temperatures, in which Complex 1 corresponded to the global minima and Complex 3 being the first higher energy local minimum at B3LYP/6-311G++(d,p). But, at M062x/6-311G++(d,p) Complex 1 and 3 corresponded to the higher energy local minima. The other computed complex, Complex2 which was not observed experimentally, might be present in the matrix but its identification through vibrational shifts were not possible as computationally there was no significant shift from the vibrational frequencies of Phac-D and Methanol submolecules, but energy calculations does not rule out its existence. At M062x/6-311G++(d,p), Complex 3 and 4 onnly differ by the orientation of the methyl group of methanol.

Similarly, the interaction between Phac-D and Methylamine was studied in N₂ and Ar matrix. Experimentally, two hydrogen bonded complex were observed, which was

evidenced by the shifts in the vibrational frequencies of Phac-D and Methylamine submolecules. The computations indicated three minima for the Phac-D and Methylamine adduct, but only two adduct were experimentally identified, where the structure of Complex 1 was the global minima and Complex 3 was the local minimum. The identification of Complex 2 was not possible because there was no vibrational shifts computationally, but energy calculations does not rule out the possibility of its existence.

The experimental results showed that when switching from O-H to N-H group in the interaction with Phac-D, a strong interaction for Complex 1 was observed in both cases, where C-D group of Phac-D interacted with O of Methanol and N of Methylamine. A strong interaction between acetylenic π and O-H of Methanol was also observed, but in case of N-H of Methylamine this interaction was not so strong and was evidenced by the change in dipole of $C\equiv C$ stretch only.

5.1 Scope for Future work

The work described in this thesis pertains to the study of hydrogen bonding interactions in phenylacetylene. The study of the nature of interaction of phenylacetylene when switching from O-H to N-H group can be further studied by using the derivatives of phenylacetylene containing electron withdrawing groups and electron donating groups.

BIBLIOGRAPHY

1. M. L. Huggins, 50 years of hydrogen bond theory, *Angew. Chem. Int. Ed.*, 10, 147-151 (1971).
2. G. A. Jeffrey, W. Saenger, *Hydrogen Bonding in Biological Structures*, Springer, 1991.
3. D. J. Sutor, The C-H...O hydrogen bonds in crystals, *Nature*, 195, 68-69 (1962)
4. D. J. Sudor, Evidence for the existence of C-H...O hydrogen bonds in crystals, *J. Chem. Soc.*, 1105-1110 (1963)
5. L. M. Epstein, and E. S. Shubina, New types of hydrogen bonding in organometallic chemistry, *Coordin. Chem. Rev.*, 231, 165-181 (2002).
6. L. M. Epstein, N. V. Belkova, E. I. Gutsul, E. S. Shubina, Spectral features of unconventional hydrogen bonds and proton transfer to transition metal hydrides, *Polish. J. Chem.*, 77, 1371-1383 (2003)
7. R. Custelcean and J. Jackson, Dihydrogen bonding: structures, energetics and dynamics, *Chem. Rev.*, 101, 1963-1980 (2001)
8. P. Hobza and v Spirko, Anti-hydrogen bond in the benzene dimer and other carbon proton donar complexes, *J. Phys. Chem. A.*, 102, 2501-2504(1998)
9. S. J. Grabowski, W. A. Sokalski and J. Leszczynski, is a pi...H...pi complex hydrogen bonded? , *J. Phys. Chem. A*, 108, 1806-1812 (2004)
10. X. Y. Hao, Z. R. Li, D. Wu, Y. Wang, Z. S. Li and C. C Sun, *J. Chem. Phys.*, 118, 83-86 (2003)
11. B. Q. Wang, X. Y. Hao, Z. R. Li, D. Wu, R. J. Li and C. C Sun, *Chem. Phys. Lett.*, 375, 91-95 (2003)
12. G. C. Pimentel, A. L. McClellan, *the Hydrogen Bond*, Freeman, San Francisco, 1960.

13. G. R. Desiraju, Hydrogen bridges in crystal engineering: interactions without borders, *Acc. Chem. Res.* 35, 565–573 (2002).
14. G. A. Jeffrey and W. Saenger, *Hydrogen Bonding in Biology and Chemistry* (Springer-Verlag, Berlin, 1991).
15. G. A. Jeffrey, *An Introduction to Hydrogen Bonding* (Oxford University Press, New York, 1997).
16. A. E. Reed, L. A. Curtiss, and F. Weinhold, Intermolecular interactions from a natural bond orbital, donor-acceptor viewpoint, *Chem. Rev.* 88, 899–926 (1988).
17. K. Muller-Dethlefs and P. Hobza, Noncovalent interactions: a challenge for experiment and theory, *Chem. Rev.* 100, 143–168 (2000).
18. S. Grabowski (ed.), *Hydrogen Bonding—New Insights*, 2006 Springer.
19. Robert Sedlak, Pavel Hobza, and G. Naresh Patwari, *J. Phys. Chem. A* 2009, 113, 6620–6625
20. Surajit Maity, Mridula Guin, Prashant Chandra Singh, and G. Naresh Patwari, *ChemPhysChem* 2011, 12, 26 – 46
21. CHAPTER 17, Matrix Isolation, THOMAS BALLY, Department of Chemistry, University of Fribourg, CH-1700, Fribourg, Switzerland
22. E. Whittle, D. A. Dows, G. C. Pimentel, *J. Chem. Phys.* 1954, 22, 1943.
23. M. J. Almond, K. S. Wiltshire, *Annual Reports on the Progress of Chemistry, Section C: Physical Chemistry* 2001, 97, 3
24. Matthew Robert White, MSc. Thesis, Queen’s University, Canada (2009)
25. *Matrix Isolation: A Technique for the Study of Reactive Inorganic Species*, Stephen Cradock, A. J. Hinchcliffe, Cambridge University Press, 2009
26. Owen Byrne, PhD Thesis, NUI Maynooth, Ireland (2010)
27. Hallam, H. E. *Vibrational Spectroscopy of Trapped Species* (Wiley Inter science Publication, London, 1973)
28. Pimentel, G. C; Charles, S. W. *Pure and Appl. Chem.* 1963, 7, 111
29. Buckingham, A. D. *Proc. Roy. Soc. (London) A* 1958, 248, 169
30. M.T. Bowera, G. I. Kerley, W.H. Flygare, *J. Chem. Phys.*, 1966, 45, 3399
31. D. W. Robinson, *J Chem. Phys.*, 1963, 39, 3430
32. M.T. Bowera, W.H. Flygare, *J. Chem. Phys.*, 1966, 45, 44, 1389
33. F.T. Prochaska, L. Andrews, *J. Chem. Phys.*, 1977, 67, 1139
34. K. Sundararajan, K.S. Viswanathan, *J. Mol. Struct.*, 2006, 798, 109

- K. V. J. Jose, S. R. Gadre, K. Sundararajan, K. S. Viswanathan, *J. Chem. Phys.*, 2007, 127, 104501
35. <http://www.arscryo.com/TechNotes/CryocoolerPrincipleofOperation>
36. <http://www-inst.eecs.berkeley.edu/~ee143/fa10/lab/vacuum.pdf>
37. Spectroscopy in Inorganic Chemistry, Volume 1, edited by C.N.R. Rao
38. <http://www.2spi.com/catalog/vac/santovac-5-diffusion-pump-fluid-technical-paper>
39. Gaussian 09, Revision A.1, Frisch, M. J.; Trucks, G. W.; Schlegel, H. B.; Scuseria, G. E.; Robb, M. A.; Cheeseman, J. R.; Scalmani, G.; Barone, V.; Mennucci, B.; Petersson, G. A.; Nakatsuji, H.; Caricato, M.; Li, X.; Hratchian, H. P.; Izmaylov, A. F.; Bloino, J.; Zheng, G.; Sonnenberg, J. L.; Hada, M.; Ehara, M.; Toyota, K.; Fukuda, R.; Hasegawa, J.; Ishida, M.; Nakajima, T.; Honda, Y.; Kitao, O.; Nakai, H.; Vreven, T.; Montgomery, Jr., J. A.; Peralta, J. E.; Ogliaro, F.; Bearpark, M.; Heyd, J. J.; Brothers, E.; Kudin, K. N.; Staroverov, V. N.; Kobayashi, R.; Normand, J.; Raghavachari, K.; Rendell, A.; Burant, J. C.; Iyengar, S. S.; Tomasi, J.; Cossi, M.; Rega, N.; Millam, J. M.; Klene, M.; Knox, J. E.; Cross, J. B.; Bakken, V.; Adamo, C.; Jaramillo, J.; Gomperts, R.; Stratmann, R. E.; Yazyev, O.; Austin, A. J.; Cammi, R.; Pomelli, C.; Ochterski, J. W.; Martin, R. L.; Morokuma, K.; Zakrzewski, V. G.; Voth, G. A.; Salvador, P.; Dannenberg, J. J.; Dapprich, S.; Daniels, A. D.; Farkas, Ö.; Foresman, J. B.; Ortiz, J. V.; Cioslowski, J.; Fox, D. J. Gaussian, Inc., Wallingford CT, 2009
40. Lewars, E. Computational Chemistry: Introduction to the theory and applications of molecular and quantum mechanics. Kluwer Academic Publishers, 2003
41. Essentials of Computational Chemistry: Theories and Models, Second Edition, Christopher J. Cramer
42. Hartree, D. R. 1928. *Proc. Cambridge Phil. Soc.*, 24, 89, 111, 426.
43. Hohenberg, P.; Kohn, W. *Phys. Rev. B* 1964, 136, 864
44. Parr, R. G.; Yang, W. *Density Functional Theory of Atoms and Molecules*; Oxford University Press: New York, 1989.
45. Dreizler, R. M.; Gross, E. K. V. *Density Functional Theory*; Springer: Berlin, 1990.
46. A. D. Becke, *Phys. Rev. A*, 1989, 38, 3098.
47. A. D. Becke, *J. Chem. Phys.*, 1983, 98, 5648.
48. Boys, S. F.; Bernadi, F.; *Mol. Phys.* 1970 , 19, 553

49. R. F. W. Bader, *Atoms in Molecules. A Quantum Theory*, Clarendon Press, Oxford, 1994
50. http://www.chemistry.mcmaster.ca/aim/aim_2.html